Received: 30 November 2021 | Revised: 25 February 2022 | Accepted: 9 March 2022

DOI: 10.1111/jmg.12662

ORIGINAL ARTICLE

Journal of METAMORPHIC GEOLOGY WILEY

Predicting and explaining crystallographic orientation relationships of exsolved precipitates in garnet using the edge-to-edge matching model

Duncan S. Keller[1,2] | **Jay J. Ague**[1]

[1]Department of Earth and Planetary Sciences, Yale University, New Haven, Connecticut, USA

[2]Department of Earth, Environmental and Planetary Sciences, Rice University, Houston, Texas, USA

Correspondence
Duncan S. Keller, Department of Earth, Environmental and Planetary Sciences, Rice University, 6100 Main St., Houston, TX 77005, USA.
Email: dsk7@rice.edu

Funding information
US National Science Foundation Directorate of Geosciences, Grant/Award Numbers: EAR-1753553, EAR-1250269, EAR-0744154; Yale University

Handling Editor: B. Cesare

Abstract

Relative alignments of mineral exsolutions and their host crystals can be described by crystallographic orientation relationships (COR). Exsolved phases in garnet from high-grade metamorphic rocks and igneous rocks may have COR, but the complexity of COR distributions has thus far restricted their use to identifying exsolved phases. Classification of COR also remains mineral-specific, leaving doubt as to what information COR preserve. To test how COR may be standardized, we calculated mismatch of low-index crystallographic planes (*d-value* ratios) and crystallographic directions (rows of atoms) between precipitates and garnet and defined search criteria for structural alignments likely to be energetically favourable. We analysed published electron backscatter diffraction (EBSD) data for apatite, rutile, ilmenite, corundum, and quartz precipitates in garnet ($n_{tot} = 1{,}296$) for the presence of these alignments. Our method predicts between 88% and 98% of observed alignments across the studied minerals and requires only calculations using unit cell parameters. We further show that each exsolved mineral forms COR predicted by the edge-to-edge matching model which was developed to describe unambiguous exsolution textures in alloys. Edge-to-edge matching aligns atoms at the host–precipitate interface by parallelism or near-parallelism of crystallographic planes of similar spacing and parallelism of crystallographic directions (rows of atoms) of similar length on the edges of those planes. Edge-to-edge matches likely facilitate coherent to semi-coherent interfaces by lowering surface free energy and strain energy, stabilizing precipitates. These matches are defined by criteria applicable to all minerals, making them an ideal tool for classifying, discovering and interpreting COR of diverse precipitates in garnet. This approach may also predict COR in other geological mineral pairs (e.g., exsolved feldspars). We find that edge-to-edge matching may explain the stability of the needle-shaped morphologies commonly observed for exsolution textures in garnet. Edge-to-edge matching COR distributions can be tested as proxies of the state of the host rock at the time of exsolution to evaluate factors such as temperature, cooling rate, degree of undercooling, and/or strain. Patterns of edge-to-edge matching COR may be paired with

geothermobarometry and/or petrochronology to provide a powerful new tool for studying the histories of granulite and eclogite facies metamorphic and igneous rocks.

KEYWORDS
COR, edge-to-edge matching, exsolution, garnet, precipitate

1 | INTRODUCTION

Exsolution phenomena are useful petrological tools because the resulting mineral textures preserve information about a rock's pressure–temperature (*P*–*T*) path within the Earth. The extent to which petrogenetic information can be retrieved from exsolution textures in different minerals varies, however. Garnets from high-grade metamorphic rocks and some igneous rocks may contain a spectrum of inequidimensional microinclusions ranging from flattened lamellar shapes (including plates) to elongated rods and finally to highly elongated acicular needles. We refer to this spectrum of shapes as Lamellar to Acicular Microinclusions (LAMs). In garnet, LAMs tend to have distinctive shape-preferred orientation (SPO), most commonly parallel to $<111>_{garnet}$, and three-dimensional distribution within the host garnet as isolated crystals; those that can be seen using a petrographic microscope are generally ~500 nm to 10 μm wide and up to ~800 μm long (e.g., Figure 1).

A growing body of work has developed and debated the nature of LAMs in garnet as exsolution textures that can be used as petrogenetic indicators in rocks for which conventional geothermobarometers record retrogressed conditions. The longstanding consensus in geoscience is that LAMs in garnet form by exsolution and represent, partially or wholly, chemical components stable in the garnet structure at elevated pressure and/or temperature. Strong chemical and crystallographic evidence underlies the exsolution hypothesis. Chemical evidence includes the connection between LAM chemistry and substitutions in the garnet structure and the association of LAMs with high-grade metamorphism and/or upper mantle conditions (Ague et al., 2013; Alifirova et al., 2015; Aulbach, 2020; Haggerty & Sautter, 1990; Keller & Ague, 2019; Keller & Ague, 2020; Mposkos & Kostopoulos, 2001; Sakamaki et al., 2016; Shinevar et al., 2021; Song et al., 2005; Spengler, 2006; Spengler et al., 2021; van Roermund et al., 2000; van Roermund & Drury, 1998; Xu & Wu, 2017; Zhang et al., 2011; Zhang & Liou, 1999). In cases where garnet has experienced arrested diffusional relaxation, depletion halos of precipitate-forming components in the host garnet are observed (Ague & Axler, 2016; Ague & Eckert, 2012; Axler & Ague, 2015). Crystallographic evidence includes the presence of crystallographic orientation relationships (COR) between LAMs and garnet (Keller & Ague, 2019; Keller & Ague, 2020; Proyer et al., 2013; Song et al., 2005; Spengler, 2006; Xu & Wu, 2017; Zhang et al., 2011) and the unusual habits of some LAM minerals such as rutile needles elongated along $<103>_{rutile}$ rather than the *c*-axis (Griffin et al., 1971; Proyer et al., 2013), as well as

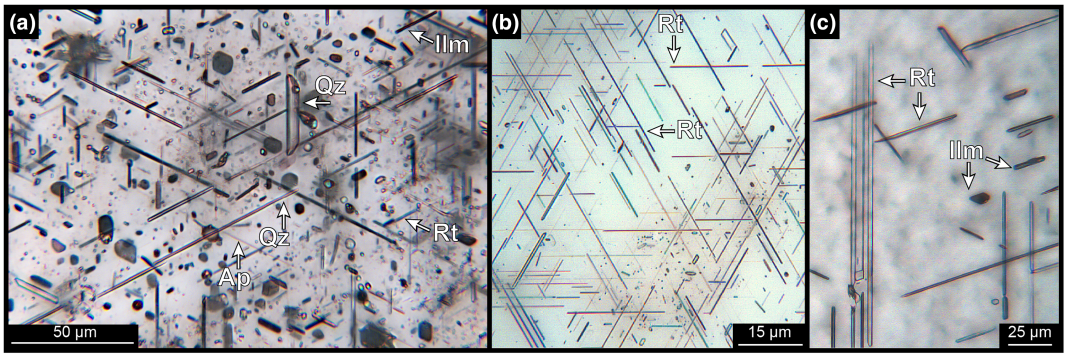

FIGURE 1 Thin section photomicrographs of oriented precipitates in metamorphic garnet from the Brimfield Schist, CT, USA. (a) Quartz (Qz), ilmenite (Ilm), apatite (Ap) and rutile (Rt) lamellar to acicular microinclusions (LAMs) (sample JAQ335A-2). Note small, equant morphologies accompanying larger needles and plates. (b) Fine rutile LAMs in thin section viewed parallel to $<111>_{garnet}$ (sample JAQ341B-5). (c) Coarse rutile and ilmenite precipitates (sample JAQ27-5). Images are taken in plane-polarized light with extended depth of field to maintain focus throughout the depth of the thin section

ilmenite (Keller & Ague, 2019) and quartz (Keller & Ague, 2020) LAMs elongated along an *a*-axis rather than the *c*-axis. These traits are extremely unusual for examples of these minerals in rock matrices but may be quite common in LAM textures. In part because of these strong lines of evidence, and in part because of evidence resulting from the results of this study, we refer to LAMs in this work as precipitates.

Rutile, ilmenite and apatite are the most common LAMs in garnet and are recognized from diverse granulite, high-pressure granulite and eclogite facies rocks (e.g., Axler & Ague, 2015; Keller & Ague, 2018; Keller & Ague, 2019; Proyer et al., 2013). Pyroxene, quartz, amphibole, and mica LAMs are interpreted as decomposition products of majoritic garnet in ultrahigh-pressure (*UHP*) rocks, in some cases with rutile, ilmenite and apatite precipitates (Alifirova et al., 2015; Haggerty & Sautter, 1990; Keller & Ague, 2020; Mposkos & Kostopoulos, 2001; Sakamaki et al., 2016; Song et al., 2005; van Roermund & Drury, 1998; Xu & Wu, 2017; Zhang et al., 2011).

In this work, we use the term 'exsolution' to encompass the variety of unmixing processes that result in diffusion-mediated precipitation of a new phase derived wholly or in part from chemical components of the precursor grain. This may be closed-system exsolution, such as is observed in alloys (e.g., Bunge et al., 2003; Howe, 1997; Nabarro, 1940; Shewmon, 1969), discontinuous precipitation (e.g., Cahn et al., 1979; Thomas & Nachlas, 2020) or open-system precipitation (Adegoke et al., 2021; Keller & Ague, 2020; Proyer et al., 2013). The common thread uniting these processes is that the exsolved phases nucleate within the host grain and comprise components largely or wholly sourced from the precursor grain that can be directly linked to solid solution components of the precursor. Controlled laboratory experiments on sulfides make it unambiguously clear that a completely closed system is not a prerequisite for the solid-state precipitation of mineral phases from a host to form oriented precipitates (Adegoke et al., 2021). Spinodal decomposition is another form of exsolution (e.g., Abart et al., 2009; Sánchez-Muñoz et al., 2016) but is not considered herein because it does not involve precipitate nucleation.

Metallurgical studies of anthropogenic alloys and meteorites offer several angles of comparison for studying exsolution of precipitates from garnet. Precipitates may be produced in alloys on timescales of hours to days, allowing for controlled study of exsolution textures with unambiguous origins. Metallurgy, mineralogy and petrology make use of a common body of analytical tools such as scanning electron microscopy (SEM), electron backscatter diffraction (EBSD) and transmission electron microscopy (TEM) to study deformation and exsolution processes. Criteria for defining COR in alloys are applicable to rock-forming minerals, and observations of exsolution in alloys and models of the influence of factors such as cooling rate and strain upon precipitate characteristics such as shape and COR have clear applicability to exsolution in geological systems. Studies of exsolution textures in meteorites provide a complementary natural laboratory for examining exsolution in systems with slower cooling rates than those achieved in laboratory experiments (e.g., Bunge et al., 2003).

In this work, we briefly outline the underlying energetics of precipitate growth and their effects on COR formation and summarize COR classification systems for LAMs in garnet. We introduce for geological consideration the edge-to-edge matching model (Kelly & Zhang, 2006; Zhang & Kelly, 1998; Zhang & Kelly, 2005) developed for explaining COR in alloys and present results for its application to LAMs in garnet as a unified COR classification system. We discuss several factors that may affect edge-to-edge matching COR formation and discuss how edge-to-edge matching COR of precipitates in garnet may be developed to recover information about the physical state of the host rock during exsolution that might otherwise be inaccessible.

2 | BRIEF REVIEW OF PRECIPITATION ENERGETICS

The solid-state formation of a precipitate in a crystalline medium and that precipitate's COR are controlled by thermodynamic and kinetic factors. The energetics of nucleation are described by the generalized expression (e.g., Cahn, 1957; Wilson & Partridge, 1965):

$$\Delta G_{\text{growth}} = \Delta G_{\text{volume}} + \Delta G_{\text{surface}} + \Delta G_{\text{strain}}. \quad (1)$$

ΔG_{volume} is the volume free energy change of precipitation. This term is negative if the precipitate is stable as a new phase and becomes more negative as the host is supersaturated with respect to precipitate-forming components (Cahn, 1957). $\Delta G_{\text{surface}}$ is the free energy of the host–precipitate interface and is always positive because a new interface must be created as exsolution begins. Boundaries that match similar structures of atoms between precipitate and host have smaller values of $\Delta G_{\text{surface}}$ because repulsive forces are minimized and there are fewer broken bonds and defects than at a mismatched boundary. ΔG_{strain} is the energy required to form a structurally matched boundary between precipitate and host by distorting bonds across or near the interface. This term can be larger or smaller depending on elastic interactions between host and precipitate(s)

(e.g., Cahn, 1957; Russell, 1980). ΔG_{strain} also encompasses effects from the shape of the precipitate (e.g., Nabarro, 1940) and effects from the volume change produced by precipitation, which would be accommodated by strain in the host lattice around the precipitate. In order for ΔG_{growth} to be negative and favour exsolution, ΔG_{volume} must be more negative than $\Delta G_{surface} + \Delta G_{strain}$. The classical approach we outline here, which stems from Gibbs (1878), is intended to serve as a generalized introduction to the major factors generally thought to influence nucleation behaviour in crystalline solids; these factors form a basis for interpreting nucleation and growth of exsolved precipitates. Quantitative approaches to evaluating the magnitudes and relative importance of these factors are areas of ongoing study, and new factors may yet be discovered.

Nucleation may broadly be subdivided into two types. Homogeneous nucleation of precipitates proceeds in the absence of interactions with host microstructures such as grain boundaries or dislocations. Heterogeneous nucleation is the nucleation of a precipitate on a pre-existing structure such as a dislocation or a heterophase boundary (e.g., between the host and another inclusion). Heterogeneous nucleation lowers the energetic barrier to nucleation because it does not require the formation of a new boundary or dislocation within the host and should be kinetically favourable if appropriate sites are available in the system (e.g., Cahn, 1957). Both homogeneous (e.g., Baumann & Williams, 1985; Chawla et al., 1991; Russell, 1980; Servi & Turnbull, 1966) and heterogeneous (e.g., Chawla et al., 1991; Cho et al., 2002; Qiu et al., 2007; Russell, 1980; Wilson & Partridge, 1965) nucleation have been demonstrated experimentally in alloys. Heterogeneous nucleation of rutile precipitates at migrating quartz grain boundaries has also been produced in a laboratory setting (Thomas & Nachlas, 2020). Host structures existing prior to precipitate exsolution, such as overgrown inclusions, dislocations from strain, dislocations from growth, or point defects would be expected to influence heterogeneous nucleation behaviour in rock-forming minerals.

Orientations of solid-state precipitates that facilitate good atomic matching across the host–precipitate interface are thought to form preferentially because of their role in reducing the free energy of the system (e.g., Christian, 2002). A precipitate that shares bonds with the host across the interface is said to be 'coherent'. By the strictest definition, coherency requires uninterrupted alignment of host and precipitate structures, so some authors distinguish 'semi-coherent' boundaries, which have regions of coherent bond sharing at the interface separated by dislocations and/or interfacial ledges (e.g., Dahmen & Westmacott, 1983; Phillips et al., 1980b; Smith & Shiflet, 1987; Weatherly, 1971; Weatherly & Nicholson, 1968). Both of these families of structures create offsets at the host–precipitate interface that accommodate elastic energy.

The traditional approach in metallurgy is to report the quality of fit between two crystal structures as a percentage difference, usually termed 'misfit'. The term 'mismatch' is also sometimes used, in some cases somewhat interchangeably with 'misfit' (e.g., Smith & Shiflet, 1987; Winkelman et al., 2007; Zhang & Kelly, 1998). In this work, we use the term 'mismatch' to denote the absolute gap between the aligned features (e.g., two lattice planes) and the term 'misfit' to denote a percentage difference.

Estimates of a misfit threshold which still allows for a favourable structural match vary from 4% (Griffiths et al., 2016; Servi & Turnbull, 1966) to up to 10%; even with ~10% misfit, common COR with semi-coherent matching in metallic systems may still form (Zhang & Kelly, 2005). A precipitate may be coherent in one or more directions but not in others (e.g., Bailey, 1963; Howe et al., 1985; Phillips et al., 1980a). Coherency affects precipitate growth because precipitates with coherent interfaces achieve lower interfacial energy than incoherent precipitates by sharing bonds (Cahn, 1957; Servi & Turnbull, 1966; Smith & Shiflet, 1987).

In this work, we use the term 'periodic structural matching' to denote an interface with compatible structural elements (e.g., crystallographic planes and crystallographic directions representing rows of atoms) aligned so that bonds are shared at regular intervals and some degree of structural continuity is achieved between precipitate and host. Dislocations or interfacial ledges are a likely accommodation mechanism to form such an interface, but we define this concept in a general sense without hypothesizing a particular mechanism for accommodating misfit that must apply in all cases. For host–precipitate pairs representing two different crystal systems and oxygen sublattices, such as garnet and rutile, periodic structural matching accommodated by dislocations, interfacial ledges and/or strain may be the highest degree of fit that is geometrically possible.

Detailed formulations of nucleation energetics for the diverse precipitate suites reported in garnet would be extremely challenging to resolve quantitatively. Even in the simplest case of a matrix and a precipitate with the same elastic constants, the expression describing the free energy of formation of an incoherent precipitate nucleus on a dislocation becomes a second-order, nonlinear partial differential equation requiring a numerical solution (Gómez-Ramírez & Pound, 1973). Moreover, for garnet and a complex suite of precipitates with diverse crystal structures, numerical solutions will become far more challenging than this. What is clear is that the interfacial

energetics ($\Delta G_{surface}$ and ΔG_{strain}) of the host and precipitate structures must affect COR development because they describe the energy of the contact between precipitate and host (e.g., Habler & Griffiths, 2017). Although the structures of garnet and its most common precipitates have inherent geometric differences, small mismatches could be accommodated by strain and/or dislocations to produce periodic structural matching (e.g., Smith & Shiflet, 1987; Weatherly & Nicholson, 1968).

3 | COR BACKGROUND

3.1 | COR in garnet

Studies of the COR between exsolved precipitates and their host garnets have revealed that for a given exsolved mineral, some COR are recognized from numerous localities (e.g., Keller & Ague, 2019; Xu & Wu, 2017; Zhang et al., 2011). Complex distributions of relationships may exist even from the same locality, however, and LAMs inferred to have exsolved may also lack discernable COR. Thus, COR formation mechanisms remain poorly understood, especially the reasons for the different distributions of COR noted from different localities. The needle- and plate-like shapes of precipitates indicate, however, that they have experienced little to no recrystallization, because these forms have high surface area to volume ratios and would readily recrystallize to more spherical or equant morphologies (Cesare et al., 2021). Moreover, no study of garnet–LAM COR has recognized discrete domains within one garnet with different orientations that would require collection or analysis of separate datasets.

Garnet–LAM COR presented to date can be broadly classified based on the number of aligned structural elements (crystallographic planes or directions) between the LAM and host garnet (Habler & Griffiths, 2017). A 'specific' COR fixes two structural elements between the LAM and host and therefore has no rotational degrees of freedom. A 'statistical' COR fixes one set of structures and allows one rotational degree of freedom and/or spread of alignments (dispersion) around an axis of matching. Specific and statistical COR are useful for classifying COR data, but these definitions are independent of the nature of the phase interface.

Although COR have been used to argue that LAMs are exsolved from garnet, the lack of a straightforward and efficient approach for understanding COR formation derived from broadly applicable principles has thus far limited the development of COR as petrogenetic indicators beyond their use for fingerprinting precursor garnet chemistry (e.g., Keller & Ague, 2020; Zhang et al., 2011). No study to date has defined broadly applicable criteria for predicting COR of diverse exsolved minerals in garnet. Furthermore, different classification schemes for COR of the same exsolved mineral have been presented in different studies. Interpretation of COR results has therefore been restricted to comparing (and often re-classifying) results for the same mineral between localities. This approach has demonstrated that precipitates show locality-specific differences, but does not allow for detailed study of the information preserved by different precipitate minerals, and restricts opportunities to compare two localities that do not share the same suite of precipitates. A more systematic and uniform approach would greatly expand the utility of COR datasets.

3.2 | Predicting COR using the edge-to-edge matching model

Various salient features of COR in metallurgical systems, such as the alignment of close-packed crystallographic planes (e.g., Bunge et al., 2003; Stanford & Bate, 2005) and/or close-packed crystallographic directions (e.g., Bunge et al., 2003; Shiflet & van der Merwe, 1994) at the host–precipitate interface have been tested to explain the formation of COR in alloys. Neither of these traits is necessarily observed for all COR, however (e.g., Dahmen, 1982; He et al., 2006; Shiflet & van der Merwe, 1994), leaving uncertainty as to how to predict COR formation in metals. A proposed solution is the edge-to-edge matching model (Kelly & Zhang, 2006; Zhang & Kelly, 1998; Zhang & Kelly, 2005). The edge-to-edge matching model was developed for solid-state phase transformations and posits that parallelism or near parallelism of crystallographic planes with similar *d-values* and parallelism of crystallographic directions of similar length within those planes allows bonds to be shared efficiently along the host–precipitate interface. Crystallographic directions are vectors representing the distance between repeating atomic positions in the crystal structure. For example, Ti atoms at the origin positions of rutile unit cells can be connected by a vector along the rutile *c*-axis with magnitude of 2.96 Å (at 298 K and 1 bar). We thus use the notation $[001]_{rutile} = 2.96$ Å.

Edge-to-edge matching is hypothesized to produce a low-energy, coherent or semi-coherent structural match that favours COR that reduce the free energy of the host–precipitate system (e.g., Kelly & Zhang, 2006; Liu et al., 2020; Qiu et al., 2007). If edge-to-edge matching reduces $\Delta G_{surface}$ during the initial formation of the precipitate nucleus by facilitating bond sharing and aligning the most structurally similar crystallographic planes and directions of host and precipitate, this should help stabilize the exsolved phase. Similarly, alignment of similarly

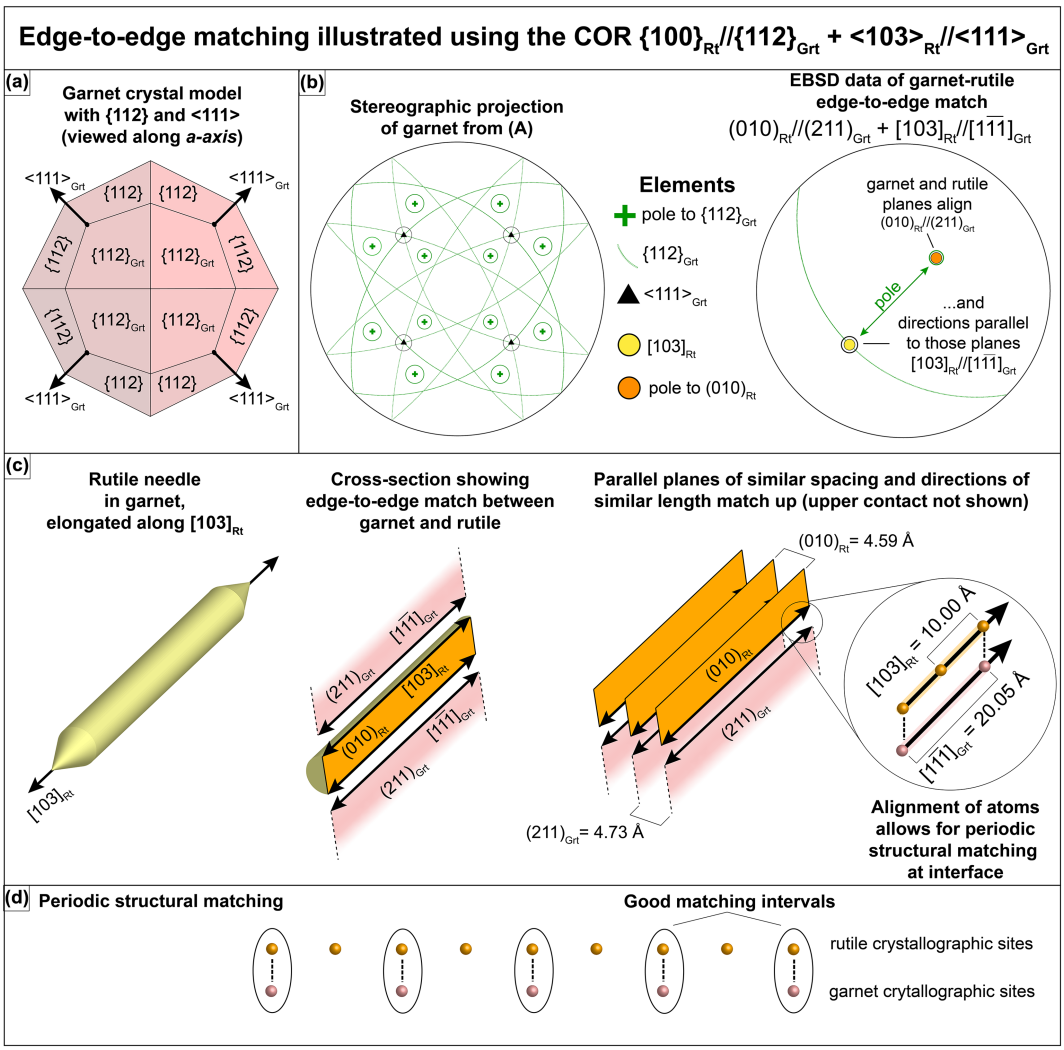

FIGURE 2 Illustration of an edge-to-edge matching crystallographic orientation relationship (COR) using an example from this study. The COR is given both in generalized form and using specific indices for a single needle (see Section 4). (a) Trapezohedral garnet crystal model showing the planes (represented as crystal faces) and directions relevant to the example COR. (b) Equal-angle, upper hemispheric stereographic projections of the garnet crystal in Panel (a) and an electron backscatter diffraction (EBSD) analysis of a rutile lamellar to acicular microinclusion (LAM) with the example COR. Rutile structures overlap with matching garnet structures. (c) Schematic illustration of edge-to-edge matching at the host–precipitate interface. Matches form along plane edges inside the garnet structure. Edge-to-edge matching allows for periodic structural matching by bond sharing across the phase boundary. The rutile needle is drawn as a generalized cylinder for simplicity because rutile needles may show diverse facets (e.g., Hwang et al., 2016). (d) Schematic illustration of periodic structural matching based on that observed in edge-to-edge matches produced in laboratory settings (e.g., Hay, 2007; Liu et al., 2020)

spaced crystallographic planes during nucleation should reduce ΔG_{strain} because ratios of interplanar spacing close to unity lower the elastic strain of the match (e.g., Howe, 1997). This likely allows for semi-coherent to coherent lattice matching. Numerous common COR in alloys, including COR in Widmanstätten patterns, undoubtedly formed by exsolution processes in cooling meteorites, satisfy the edge-to-edge matching model (Kelly & Zhang, 2006; Zhang & Kelly, 2005; Zhong et al., 2011). Edge-to-edge matching can also notably predict COR of precipitates heterogeneously nucleated on additive particles (Easton et al., 2016; Qiu et al., 2007) and can predict the multiple COR observed in some systems (e.g., Hay, 2007). Furthermore, edge-to-edge matches have been imaged directly using TEM (e.g., Liu et al., 2020). Edge-to-edge matching is commonly observed between close-packed directions and planes but may also be observed for structural elements that are not close-packed (e.g., Zhong et al., 2011). The predictive value and generalized framework of the edge-to-edge matching model makes it an ideal candidate for predicting COR of precipitates in garnet.

The edge-to-edge matching model may be applied by building upon established approaches used for LAMs in garnet. Previous work has shown that for some COR, parallel crystallographic directions of LAMs and garnet have similar lengths in multiples of 2:1 (rutile:garnet, Griffiths et al., 2016) and 4:1 (pyroxene:garnet, Zhang et al., 2011). Similarly, the presence of alignments found in COR datasets for rutile (Griffiths et al., 2016; Keller & Ague, 2019), apatite, ilmenite and corundum LAMs in garnet (Keller & Ague, 2019) has been explained by the matching *d-values* of similar magnitudes (in varying multiples). By definition, edge-to-edge matching requires both the presence of a *d-value* match and a direction length match parallel to the planar match (Figure 2b,c; Kelly & Zhang, 2006).

4 | DATA, SAMPLES AND METHODS

We analysed published EBSD data for five LAM minerals: apatite (Keller & Ague, 2019), ilmenite (Griffiths et al., 2016; Keller & Ague, 2019), rutile (Griffiths et al., 2016; Griffiths et al., 2020; Keller & Ague, 2019), corundum (Griffiths et al., 2016) and quartz (Keller & Ague, 2020). We chose these datasets because they are available in full and allow for thorough re-analysis of primary data. Acquisition methods for each dataset are given in the original works. We also comment on pyroxene and amphibole precipitates in garnet. We briefly outline the geologic setting of the samples below.

4.1 | Rock samples

The rocks studied by Keller and Ague (2019, 2020) are *UHP* and ultrahigh-temperature (*UHT*) gneisses from the Brimfield Schist unit of the Central Maine Terrane, USA. The field area is an Acadian/Neoacadian mélange zone that contains *UHP* (Keller & Ague, 2020) and *UHT* (Ague et al., 2013) rocks, high-pressure granulites (Keller & Ague, 2018) and hydrous ultramafic cumulates (Tassara et al., 2021).

The rocks studied by Griffiths et al. (2016, 2020) are kyanite-bearing metapegmatites from near Wirtbartl in the Austrian Alps. The metapegmatites were subjected to Cretaceous eclogite facies metamorphism and crop out as pods in crystalline Alpine basement alongside eclogites (Rogowitz & Huet, 2021). Rocks from a single locality were studied in Griffiths et al. (2016). Griffiths et al. (2020) examined a sample from the 2016 study and another from a different metapegmatite lens ~2 km away in the same unit.

4.2 | Morphologies of analysed phases

Apatite, ilmenite, rutile and quartz datasets from Keller and Ague (2019, 2020) are restricted to LAMs with SPO parallel to $<111>_{garnet}$. Ilmenite, rutile and corundum datasets from Griffiths et al. (2016) were collected in garnet cores; these LAMs are reported as having no SPO. Rutile datasets from Griffiths et al. (2020) are restricted to garnet rims and consist of 79% rutile needles with SPO parallel to $<111>_{garnet}$ and 21% rutile with other shapes.

4.3 | Crystallographic calculations and classifications

A generalized garnet composition of $Pyrope_{25}Almandine_{55}Grossular_{20}$, roughly corresponding to eclogitic garnet, was chosen. The unit cell dimension of this generalized garnet composition ($a = 11.58$ Å) was calculated as a linear combination of unit cell parameters for the pyrope, almandine and grossular endmembers (Thiéblot et al., 1998). We chose this hypothetical garnet composition to be broadly applicable to a variety of rocks; garnets from high-grade metamorphic crustal rocks will rarely differ from the unit cell parameters of this example by more than ~1%. We estimated unit cell volume for representative garnets of this study using garnet endmember unit cell parameters from Thiéblot et al. (1998) and Rodehorst et al. (2002) and the calculation method of Locock (2008) normalized for pyrope, almandine, grossular and spessartine. Garnet from Griffiths et al. (2020) has $a = \sim 11.57$ Å, and from Keller and Ague (2020) has $a = \sim 11.52$ Å; these values are within 0.5% of the chosen generalized composition. Host and LAM mineral *d-values* were calculated using standard formulations (Nesse, 2011). Lengths of crystallographic directions were calculated from a structural model in VESTA (Momma & Izumi, 2011) using the cited unit cell parameters for each LAM mineral and the generalized garnet composition (Tables 1–5). Calculations used unit cell parameters at 1 bar (10^5 Pa) and 298 K, following the method of Griffiths et al. (2016). Other temperatures and pressures could be used for this calculation. We chose 1 bar and 298 K to avoid assumptions about the pressures and temperatures of exsolution and because the unit cell parameters of minerals we consider in this study change only by small fractions at high pressures and temperatures in the absence of a phase change. The ratios of axial parameters of the minerals change by <1% at the high temperatures that are likely maxima for exsolution conditions (Table S1).

TABLE 1 Mismatch (Å) between low-index structural elements and edge-to-edge matching COR for apatite and garnet

			Apatite		
	Planes		$\{10\bar{1}0\}$ *8.12 Å*	$\{11\bar{2}0\}$ *4.69 Å*	{0001} *6.89 Å*
Garnet $Py_{25}Alm_{55}Gro_{20}$	{100}	*11.58 Å*	$3.46^{(1:1)(35.1\%)}$	$2.21^{(2:1)(21\%)}$	$2.19^{(2:1)(17.4\%)}$
	{110}	*8.19 Å*	**$0.07^{(1:1)(0.9\%)}$**	$1.19^{(2:1)(13.5\%)}$	$1.30^{(1:1)(17.2\%)}$
	{111}	*6.69 Å*	$1.43^{(1:1)(19.3\%)}$	$2.00^{(1:1)(33.5\%)}$	**$0.20^{(1:1)(2.9\%)}$**
	{112}	*4.73 Å*	$1.34^{(1:2)(15.3\%)}$	**$0.04^{(1:1)(0.8\%)}$**	$2.16^{(1:1)(37.2\%)}$
	{134}	*2.27 Å*	**$0.97^{(1:4)(11.2\%)}$**	**$0.14^{(1:2)(3.3\%)}$**	**$0.07^{(1:3)(1.2\%)}$**

			Apatite		
	Directions		$<10\bar{1}0>$ *9.37 Å*	$<11\bar{2}0>$ *9.37 Å*	<0001> *6.89 Å*
Garnet $Py_{25}Alm_{55}Gro_{20}$	<100>	*11.58 Å*	$2.21^{(1:1)(21.1\%)}$	$2.21^{(1:1)(21.1\%)}$	$2.19^{(2:1)(17.4\%)}$
	<110>	*16.37 Å*	$2.37^{(2:1)(13.5\%)}$	$2.37^{(2:1)(13.5\%)}$	$2.60^{(2:1)(17.2\%)}$
	<111>	*20.05 Å*	$1.31^{(2:1)(6.8\%)}$	$1.31^{(2:1)(6.8\%)}$	**$0.60^{(3:1)(3.0\%)}$**
	<112>	*28.36 Å*	**$0.25^{(3:1)(0.9\%)}$**	**$0.25^{(3:1)(0.9\%)}$**	**$0.82^{(4:1)(2.9)}$**
	<134>	*59.04 Å*	–	–	–

	Edge-to-edge matching COR (71% of dataset)
A (48%)	$\{10\bar{1}0\}_{Ap}//\{110\}_{Grt} + <11\bar{2}0>_{Ap}//<112>_{Grt}$ + $<0001>_{Ap}//<111>_{Grt}$ alternatively: $\{11\bar{2}0\}_{Ap}//\{112\}_{Grt} + <0001>_{Ap}//<111>_{Grt}$ alternatively: $\{0001\}_{Ap}//\{111\}_{Grt} + <11\bar{2}0>_{Ap}//<112>_{Grt}$
B (16%)	$\{11\bar{2}0\}_{Ap}//\{134\}_{Grt} + <0001>_{Ap}//<111>_{Grt}$ alternatively: $\{10\bar{1}0\}_{Ap}//\{134\}_{Grt} + <0001>_{Ap}//<111>_{Grt}$.
C (6%)	$\{0001\}_{Ap}//\{111\}_{Grt} + (1–3) <10\bar{1}0>_{Ap}//<112>_{Grt}$

Note: Bolded pairs are present in the studied datasets (dark blue shading in Figure 3). Boxed pairs form edge-to-edge matching COR (light blue shading in Figure 3). Superscripts indicate the repetition factor at which structural elements align and the percentage misfit for the alignment (van der Merwe, 1978). Mismatch values for pairs with a ≥6:1 repetition factor have been omitted. Apatite parameters are from Brunet et al. (1999), and garnet parameters are from Thiéblot et al. (1998). Abbreviations: COR, crystallographic orientation relationship; Ap, apatite; Grt, garnet.

Some studies (e.g., Fleet et al., 1980; Robinson et al., 1977) have used the angles between crystallographic axes of monoclinic pyroxene as an indicator of the temperature at which oxide precipitates exsolved. This approach demonstrates that temperature-dependent information can be preserved in, and retrieved from, petrological exsolution systems. However, this method is dependent upon either symmetry changes in clinopyroxene structures with changing temperature and miscibility gaps between augite and pigeonite (e.g., Robinson et al., 1977) or the change of clinopyroxene β angle with temperature (e.g., Fleet et al., 1980). These factors are not relevant to the minerals of this study, although they would likely be useful in detailed consideration of pyroxene exsolution from garnet.

Absolute mismatches (in Å) were calculated between low-index structural elements (crystallographic planes and directions) of LAM minerals and garnet (Tables 1–5). Reported mismatches are the smallest value for repetition factors ≤5 (i.e., coinciding every fifth repetition of the structural element). Analysed LAM structural elements are either orthogonal or parallel to the mineral's mineral unit cell axes and analysed garnet structural

TABLE 2 Mismatch (Å) between low-index structural elements and edge-to-edge matching COR for rutile and garnetMismatch (Å) between low-index structural elements and edge-to-edge matching COR for ilmenite and garnet

Rutile

Garnet $Py_{25}Alm_{55}Gro_{20}$	Planes		{100} *4.59 Å*	{110} *3.25 Å*	{001} *2.96 Å*
	{100}	*11.58 Å*	2.20(3:1)(17.3%)	1.41(4:1)(11.6%)	**0.26**(4:1)(2.2%)
	{110}	*8.19 Å*	**1.00**(2:1)**(11.4%)**	1.56(3:1)(17.4%)	**0.69**(3:1)**(8.1%)**
	{111}	*6.69 Å*	2.09(1:1)(37.2%)	**0.19**(2:1)**(2.9%)**	**0.77**(2:1)**(12.2%)**
	{112}	*4.73 Å*	**0.13**(1:1)**(3.0%)**	1.48(1:1)(37.1%)	1.19(2:1)(22.3%)
	{134}	*2.27 Å*	**0.05**(1:2)**(1.1%)**	**0.98**(1:1)**(35.5%)**	**0.69**(1:1)**(26.4%)**

Rutile

Garnet $Py_{25}Alm_{55}Gro_{20}$	Directions		<100> *4.59 Å*	<110> *6.50 Å*	<001> *2.96 Å*	<101> *5.46 Å*	<103> *10.00 Å*
	<100>	*11.58 Å*	2.20(3:1)(17.3%)	1.41(2:1)(11.6%)	**0.26**(4:1)**(2.2%)**	**0.66** (2:1)**(5.9%)**	1.58(1:1)(14.6%)
	<110>	*16.37 Å*	2.00(4:1)(11.5%)	3.11(3:1)(17.5%)	–	**0.01**(3:1)**(0.06%)**	3.62(2:1)(20.0%)
	<111>	*20.05 Å*	1.68(4:1)(8.8%)	**0.57**(3:1)**(2.8%)**	–	1.79(4:1)(8.5%)	**0.06**(2:1)**(0.2%)**
	<112>	*28.36 Å*	–	2.38(4:1)(8.7%)	–	1.06(5:1)(3.8%)	1.63(3:1)(5.6%)
	<134>	*59.04 Å*	–	–	–	–	–

	Edge-to-edge matching COR (45% of dataset)
A (13%)	$\{100\}_{Rt}//\{134\}_{Grt} + <103>_{Rt}//<111>_{Grt}$ (includes "Widmanstätten-type COR" of Keller & Ague, 2019)
A* (22%)	$\{100\}_{Rt}//\{110\}_{Grt} + <101>_{Rt}//<100>_{Grt}$
B (8%)	$\{100\}_{Rt}//\{112\}_{Grt} + <103>_{Rt}//<111>_{Grt} \pm <101>_{Rt}//<110>_{Grt}$
C (1%)	$\{100\}_{Rt}//\{110\}_{Grt} + <103>_{Rt}//<111>_{Grt}$
D (1%)	$\{001\}_{Rt}//\{110\}_{Grt} + <110>_{Rt}//<111>_{Grt}$
E (0.4%)	$\{001\}_{Rt}//\{134\}_{Grt} + <110>_{Rt}//<111>_{Grt}$
F (0.4%)	$\{100\}_{Rt}//\{112\}_{Grt} + <101>_{Rt}//<110>_{Grt}$

Note: Bolded pairs are present in the studied datasets (dark blue shading in Figure 4). Boxed pairs form edge-to-edge matching COR (light blue shading in Figure 4). Superscripts indicate the repetition factor at which structural elements align and the percentage misfit for the alignment (van der Merwe, 1978). Mismatch values for pairs with a ≥6:1 repetition factor have been omitted. Rutile parameters are from Meagher and Lager (1979), and garnet parameters are from Thiéblot et al. (1998). COR A* is designated as such because its prevalence may be a statistical artefact (see Sections 5 and 6). Abbreviations: COR, crystallographic orientation relationship; Rt, rutile; Grt, garnet.

elements are orthogonal or parallel to garnet unit cell axes and/or are 90° from $<111>_{garnet}$ (Tables 1–5). These selection criteria were chosen so that the analysed elements represent common crystallographic faces, face edges or poles to these features, on crystals of these minerals.

The EBSD data were analysed for the presence of each of the alignments with mismatch ≤1 Å. Because there are no prior data on the role of misfit in the formation of edge-to-edge matching in silicate systems, we chose a conservative cut-off of absolute mismatch (1 Å). This provides a straightforward way to compare directly many alignments that occur at different repetition intervals (e.g., 1:2 and 1:4), rather than fixing a frame of reference for percentage misfit. We analysed 62 total alignments. Our cut-off of 1 Å included 11 alignments with >10% misfit and excluded 17 alignments with <10% misfit that have mismatch >1 Å. We give the percentage misfit for each alignment, calculated using the approach of van der Merwe (1978) for bulk crystals, in Tables 1–5.

TABLE 3 Mismatch (Å) between low-index structural elements and edge-to-edge matching COR for ilmenite and garnet

			Ilmenite		
	Planes		$\{10\bar{1}0\}$ *4.41 Å*	$\{11\bar{2}0\}$ *2.54 Å*	{0001} *14.09 Å*
Garnet $Py_{25}Alm_{55}Gro_{20}$	{100}	*11.58 Å*	$1.64^{(3:1)(13.3\%)}$	$1.14^{(5:1)(9.2\%)}$	$2.51^{(1:1)(19.6\%)}$
	{110}	*8.19 Å*	**$0.63^{(2:1)(7.4\%)}$**	**$0.56^{(3:1)(7.2\%)}$**	$2.29^{(1:2)(15.0\%)}$
	{111}	*6.69 Å*	$2.13^{(2:1)(27.5\%)}$	**$0.95^{(3:1)(13.0\%)}$**	**$0.72^{(1:2)(5.2\%)}$**
	{112}	*4.73 Å*	**$0.32^{(1:1)(7.0\%)}$**	**$0.36^{(2:1)(7.1\%)}$**	**$0.10^{(1:3)(0.7\%)}$**
	{134}	*2.27 Å*	**$0.14^{(1:2)(2.9\%)}$**	**$0.27^{(1:1)(11.2\%)}$**	$2.73^{(1:5)(21.5\%)}$

			Ilmenite		
	Directions		$<10\bar{1}0>$ *5.09 Å*	$<11\bar{2}0>$ *5.09 Å*	<0001> *14.09 Å*
Garnet $Py_{25}Alm_{55}Gro_{20}$	<100>	*11.58 Å*	$1.40^{(2:1)(12.9\%)}$	$1.40^{(2:1)(12.9\%)}$	$2.51^{(1:1)(19.6\%)}$
	<110>	*16.37 Å*	$1.11^{(3:1)(7.0\%)}$	$1.11^{(3:1)(7.0\%)}$	$2.29^{(1:1)(15.0\%)}$
	<111>	*20.05 Å*	**$0.30^{(4:1)(1.5\%)}$**	**$0.30^{(4:1)(1.5\%)}$**	$5.97^{(1:1)(34.9\%)}$
	<112>	*28.36 Å*	$2.92^{(5:1)(10.8\%)}$	$2.92^{(5:1)(10.8\%)}$	**$0.19^{(2:1)(0.6\%)}$**
	<134>	*59.04 Å*	–	–	$2.69^{(4:1)(4.6\%)}$

	Edge-to-edge matching COR (58% of dataset)
A (25%)	$\{10\bar{1}0\}_{Ilm}//\{134\}_{Grt} + <11\bar{2}0>_{Ilm}//<111>_{Grt}$
B (15%)	$\{10\bar{1}0\}_{Ilm}//\{110\}_{Grt} + <11\bar{2}0>_{Ilm}//<111>_{Grt} +$ $<0001>_{Ilm}//<112>_{Grt}$
C (5%)	$\{11\bar{2}0\}_{Ilm}//\{110\}_{Grt} + <10\bar{1}0>_{Ilm}//<111>_{Grt} +$ $<0001>_{Ilm}//<112>_{Grt}$ alternatively: $\{0001\}_{Ilm}//\{112\}_{Grt} + <10\bar{1}0>_{Ilm}//<111>_{Grt}$
D (5%)	$\{10\bar{1}0\}_{Ilm}//\{112\}_{Grt} + <11\bar{2}0>_{Ilm}//<111>_{Grt}$
E (4%)	$\{11\bar{2}0\}_{Ilm}//\{112\}_{Grt} + <10\bar{1}0>_{Ilm}//<111>_{Grt}$
F (3%)	$\{11\bar{2}0\}_{Ilm}//\{134\}_{Grt} + <10\bar{1}0>_{Ilm}//<111>_{Grt}$

Note: Bolded pairs are present in the studied datasets (dark blue shading in Figure 5). Boxed pairs form edge-to-edge matching COR (light blue shading in Figure 5). Superscripts indicate the repetition factor at which structural elements align and the percentage misfit for the alignment (van der Merwe, 1978). Mismatch values for pairs with a ≥6:1 repetition factor have been omitted. Ilmenite parameters are from Wechsler and Prewitt (1984), and garnet parameters are from Thiéblot et al. (1998). Abbreviations: COR, crystallographic orientation relationship; Ilm, ilmenite; Grt, garnet.

For corundum, which lacks direction mismatches ≤1 Å with the chosen garnet composition, only the smallest mismatch of 1.02 Å was analysed.

Each EBSD dataset was rotated into a common frame of reference and analysed for matches between LAMs and garnet using the MTEX toolbox in MATLAB (Bachmann et al., 2010; Hielscher et al., 2010). A tolerance of 5° was allowed for each analysed alignment (angles between directions or plane normals). This is consistent with examples of edge-to-edge matching where the planes meeting edge to edge at the interface are close to, but not precisely, parallel (Kelly & Zhang, 2006).

Following analysis for the selected alignments, classification of edge-to-edge matching COR proceeded by identification of LAMs with one crystallographic plane and a parallel crystallographic direction aligned with one

TABLE 4 Mismatch (Å) between low-index structural elements and edge-to-edge matching COR for corundum and garnet

			Corundum		
	Planes		$\{10\bar{1}0\}$ *4.12 Å*	$\{11\bar{2}0\}$ *2.38 Å*	{0001} *13.00 Å*
Garnet $Py_{25}Alm_{55}Gro_{20}$	{100}	*11.58 Å*	$0.79^{(3:1)(6.5\%)}$	**$0.32^{(5:1)(2.7\%)}$**	$1.42^{(1:1)(11.6\%)}$
	{110}	*8.19 Å*	**$0.06^{(2:1)(0.6\%)}$**	$1.05^{(3:1)(13.7\%)}$	$3.38^{(1:2)(23.0\%)}$
	{111}	*6.69 Å*	$1.46^{(2:1)(20.8\%)}$	**$0.45^{(3:1)(6.5\%)}$**	**$0.37^{(1:2)(2.9\%)}$**
	{112}	*4.73 Å*	**$0.61^{(1:1)(13.8\%)}$**	**$0.03^{(2:1)(0.6\%)}$**	$1.19^{(1:3)(8.7\%)}$
	{134}	*2.27 Å*	**$0.42^{(1:2)(9.7\%)}$**	**$0.11^{(1:1)(4.7\%)}$**	–

			Corundum		
	Directions		$<10\bar{1}0>$ *4.76 Å*	$<11\bar{2}0>$ *4.76 Å*	<0001> *13.00 Å*
Garnet $Py_{25}Alm_{55}Gro_{20}$	<100>	*11.58 Å*	$2.06^{(2:1)(19.5\%)}$	$2.06^{(2:1)(19.5\%)}$	$1.42^{(1:1)(11.6\%)}$
	<110>	*16.37 Å*	$2.10^{(3:1)(13.6\%)}$	$2.10^{(3:1)(13.6\%)}$	$3.38^{(1:1)(22.9\%)}$
	<111>	*20.05 Å*	**$1.02^{(4:1)(5.2\%)}$**	**$1.02^{(4:1)(5.2\%)}$**	$5.94^{(2:1)(25.8\%)}$
	<112>	*28.36 Å*	–	–	$2.37^{(2:1)(8.7\%)}$
	<134>	*59.04 Å*	–	–	$7.05^{(4:1)(12.7\%)}$

	Edge-to-edge matching COR (44% of dataset)
A (35%)	$\{10\bar{1}0\}_{Crn}//\{110\}_{Grt} + <11\bar{2}0>_{Crn}//<111>_{Grt}$
B (9%)	$\{10\bar{1}0\}_{Crn}//\{134\}_{Grt} + <11\bar{2}0>_{Crn}//<111>_{Grt}$
C (1%)	$\{10\bar{1}0\}_{Crn}//\{112\}_{Grt} + <11\bar{2}0>_{Crn}//<111>_{Grt}$

Note: Bolded pairs are present in the studied datasets (dark blue shading in Figure 6). Boxed pairs form edge-to-edge matching COR (light blue shading in Figure 6). Superscripts indicate the repetition factor at which structural elements align and the percentage misfit for the alignment (van der Merwe, 1978). Mismatch values for pairs with a ≥6:1 repetition factor have been omitted. Corundum parameters are from Fiquet et al. (1999), and garnet parameters are from Thiéblot et al. (1998). Abbreviations: COR, crystallographic orientation relationship; Crn, corundum; Grt, garnet.

crystallographic plane and a parallel crystallographic direction of the host (e.g., Kelly & Zhang, 2006).

Results are presented in terms of generalized crystallographic notation, that is, {} for planar and < > for directional structural elements. An example of individualized notation for an analysis of a single example is given in Figure 2. We outline here an example of how we present edge-to-edge matching notation. Consider the edge-to-edge matching COR $\{100\}_{rutile}//\{112\}_{garnet} + <103>_{rutile}//<111>_{garnet}$ ('COR B_{rutile}'; Table 2). Each LAM with this COR has one of the symmetrically equivalent $\{100\}_{rutile}$ planes ($(100)_{rutile}$, $(\bar{1}\,00)_{rutile}$, $(010)_{rutile}$ or $(0\bar{1}\,0)_{rutile}$) parallel to one of the symmetrically equivalent$\{112\}_{garnet}$ planes. One of the $<103>_{rutile}$ directions that is parallel to the noted plane for that LAM is aligned with one of the $<111>_{garnet}$ directions that is parallel to the noted plane for the garnet. For example, edge-to-edge matching of a rutile needle with $(100)_{rutile}//(211)_{garnet}$ would require the parallel directions $[013]_{rutile}//[1\bar{1}\bar{1}]_{garnet}$ (Figure 2b). We chose to use generalized notation because there are many permutations of functionally equivalent planes and directions that can form edge-to-edge matches for the high-symmetry host–LAM pairs considered in this work. Each individual analysis that shows edge-to-edge matching behaviour was checked to ensure that it meets the geometric criteria laid out above. In rare cases, a LAM formed a match with a garnet structural element that has the same Miller index as that expected for an edge-to-edge matching COR but did not satisfy the appropriate geometric criteria. These examples are very uncommon (<5% of the all data analysed) but must be considered when identifying edge-to-edge matches. Mineral abbreviations in all tables and figures follow Whitney and Evans (2010).

TABLE 5 Mismatch (Å) between low-index structural elements and edge-to-edge matching COR for quartz and garnet

			Quartz (α)		
	Planes		$\{10\bar{1}0\}$ *4.26 Å*	$\{11\bar{2}0\}$ *2.46 Å*	{0001} *5.41 Å*
Garnet $Py_{25}Alm_{55}Gro_{20}$	{100}	*11.58 Å*	$1.19^{(3:1)(9.9\%)}$	**$0.71^{(5:1)(6.0\%)}$**	**$0.77^{(2:1)(6.8\%)}$**
	{110}	*8.19 Å*	**$0.33^{(2:1)(3.9\%)}$**	**$0.82^{(3:1)(10.4\%)}$**	$2.62^{(2:1)(27.7\%)}$
	{111}	*6.69 Å*	$1.83^{(2:1)(24.1\%)}$	**$0.69^{(3:1)(9.8\%)}$**	$1.28^{(1:1)(21.2\%)}$
	{112}	*4.73 Å*	**$0.47^{(1:1)(10.5\%)}$**	**$0.19^{(2:1)(3.9\%)}$**	**$0.68^{(1:1)(13.4\%)}$**
	{134}	*2.27 Å*	**$0.29^{(1:2)(6.4\%)}$**	**$0.19^{(1:1)(8.0\%)}$**	**$0.86^{(1:2)(17.5\%)}$**

			Quartz (α)		
	Directions		<$10\bar{1}0$> *4.91 Å*	<$11\bar{2}0$> *4.91 Å*	<0001> *5.41 Å*
Garnet $Py_{25}Alm_{55}Gro_{20}$	<100>	*11.58 Å*	$1.75^{(2:1)(16.4\%)}$	$1.75^{(2:1)(16.4\%)}$	**$0.77^{(2:1)(6.8\%)}$**
	<110>	*16.37 Å*	$1.62^{(3:1)(10.5\%)}$	$1.62^{(3:1)(10.5\%)}$	**$0.16^{(3:1)(0.9\%)}$**
	<111>	*20.05 Å*	**$0.40^{(4:1)(2.1\%)}$**	**$0.40^{(4:1)(2.1\%)}$**	$1.57^{(4:1)(7.6\%)}$
	<112>	*28.36 Å*	–	–	$1.34^{(5:1)(4.7\%)}$
	<134>	*59.04 Å*	–	–	–

	Edge-to-edge matching COR (32% of dataset)
A (12%)	$\{10\bar{1}0\}_{Qz}//\{134\}_{Grt} + <11\bar{2}0>_{Qz}//<111>_{Grt}$
B (9%)	$\{10\bar{1}0\}_{Qz}//\{112\}_{Grt} + <11\bar{2}0>_{Qz}//<111>_{Grt} + <0001>_{Qz}//<110>_{Grt}$
C (3%)	$\{10\bar{1}0\}_{Qz}//\{110\}_{Grt} + <11\bar{2}0>_{Qz}//<111>_{Grt}$
D (2%)	$\{0001\}_{Qz}//\{134\}_{Grt} + <11\bar{2}0>_{Qz}//<111>_{Grt}$
E (2%)	$\{11\bar{2}0\}_{Qz}//\{100\}_{Grt} + <0001>_{Qz}//<100>_{Grt}$
F (2%)	$\{11\bar{2}0\}_{Qz}//\{134\}_{Grt}$ or $\{0001\}_{Qz}//\{134\}_{Grt}$ $+ <10\bar{1}0>_{Qz}//<111>_{Grt}$
G (1%)	$\{10\bar{1}0\}_{Qz}//\{110\}_{Grt}$ or $\{11\bar{2}0\}_{Qz}//\{110\}_{Grt}$ $+ <0001>_{Qz}//<100>_{Grt}$
H (1%)	$\{0001\}_{Qz}//\{134\}_{Grt} + <10\bar{1}0>_{Qz}//<111>_{Grt}$
I (0.4%)	$\{11\bar{2}0\}_{Qz}//\{112\}_{Grt} + <10\bar{1}0>_{Qz}//<111>_{Grt} + <0001>_{Qz}//<110>_{Grt}$
J (0.4%)	$\{10\bar{1}0\}_{Qz}//\{110\}_{Grt} + <0001>_{Qz}//<110>_{Grt}$

Note: Bolded pairs are present in the studied datasets (dark blue shading in Figure 7). Boxed pairs form edge-to-edge matching COR (light blue shading in Figure 7). Superscripts indicate the repetition factor at which structural elements align and the percentage misfit for the alignment (van der Merwe, 1978). Mismatch values for pairs with a ≥6:1 repetition factor have been omitted. Quartz parameters are from Kihara (1990), and garnet parameters are from Thiéblot et al. (1998). Abbreviations: COR, crystallographic orientation relationship; Qz, quartz; Grt, garnet.

5 | RESULTS

To test a standardized framework for classifying and interpreting COR based on structural matching between LAMs and garnet, we applied the predictive capacity of the edge-to-edge matching model (Kelly & Zhang, 2006; Zhang & Kelly, 1998; Zhang & Kelly, 2005) to EBSD data for apatite, rutile, ilmenite, corundum and quartz LAMs. Edge-to-edge matching requires both a *d-value* match for host and LAM crystallographic planes aligned by a COR and a direction length match within those planes that brings rows of atoms into coincidence at the interface. Because the concept of edge-to-edge matching is not based upon mineral-specific criteria, it is equally applicable to all LAM species in garnet. Results can be considered both individually for each LAM species and in aggregate. All results are for the chosen generalized garnet

composition ($Py_{25}Alm_{55}Gro_{20}$). We categorize edge-to-edge matching COR for each mineral using an ordered alphabetized system with COR A representing the most common edge-to-edge matching COR (e.g., COR $A_{apatite}$), COR B representing the second-most common edge-to-edge matching COR, and so on (Tables 1–5).

5.1 | Apatite

We analysed EBSD data for 31 apatite LAMs in the Brimfield Schist samples (Keller & Ague, 2019). These apatites all have SPO parallel to $<111>_{garnet}$ and dominantly have needle or rod shapes (81%). Apatite results are given in Table 1 and Figure 3. Of the minerals considered in this study, apatite has the largest number of alignments with garnet that have mismatches ≤0.25 Å. Among the low-index structural elements we considered, apatite can form six planar alignments and four directional alignments with mismatches ≤1 Å with garnet (Table 1). All of the investigated alignments are present in the data. At least one of the planar alignments is present for 90% of the dataset, and at least one of the directional alignments is present for 87% of the dataset. The two lowest-mismatch planar alignments (in addition to higher-mismatch alignments) and the three lowest-mismatch directional alignments form

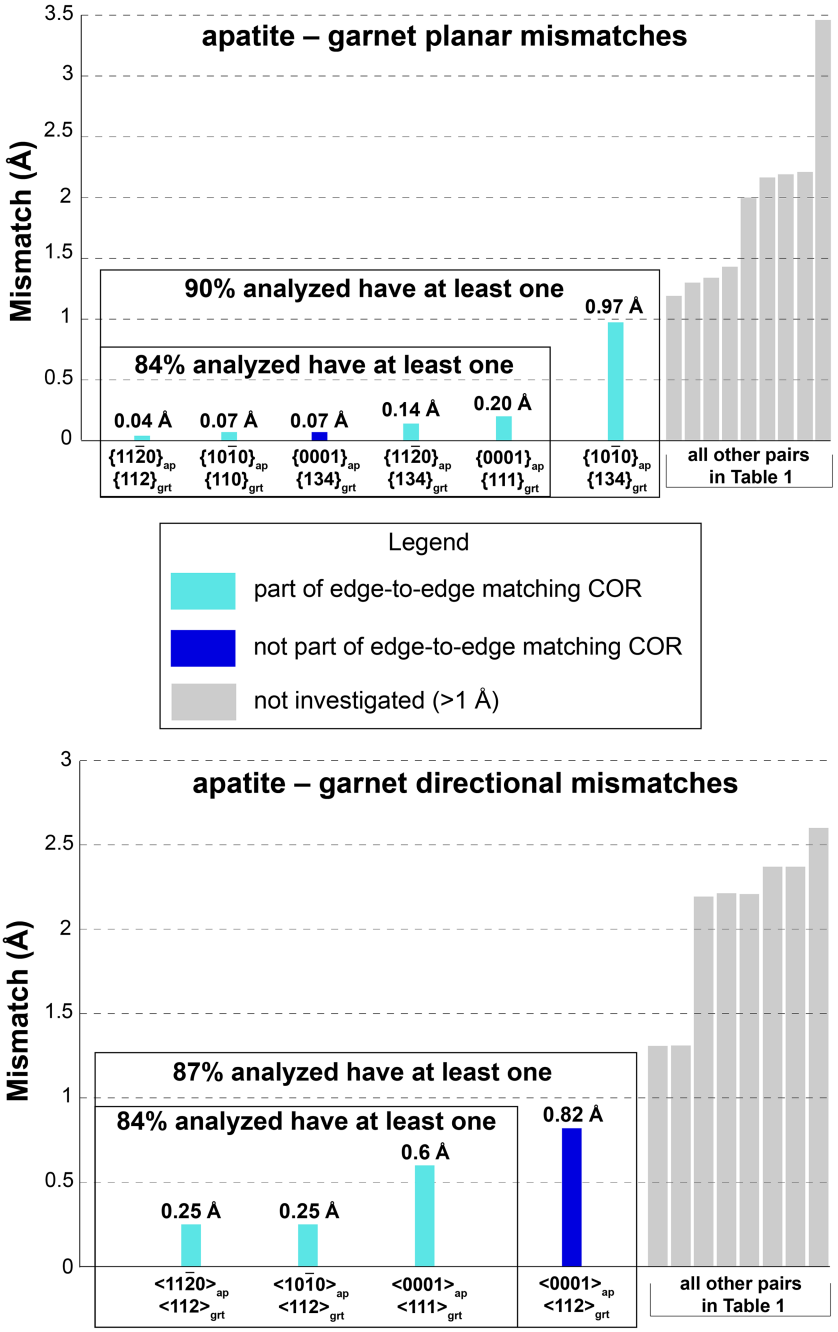

FIGURE 3 Absolute mismatch between low-index structural elements of apatite and garnet (Table 1). In total, 94% of apatites have at least one of the investigated alignments

edge-to-edge matching COR (Figure 3). Only 6% of apatites lack one of the analysed alignments. The most common apatite COR is the edge-to-edge matching COR $A_{apatite}$ (Table 1): $\{10\bar{1}\ 0\}_{apatite}//\{110\}_{garnet} + <11\bar{2}\ 0>_{apatite}//<112>_{garnet} + <0001>_{apatite}//<111>_{garnet}$. This COR constitutes a double edge-to-edge match, accounts for 48% of the dataset and can be written in several different ways to satisfy edge-to-edge matching because both $\{11\bar{2}\ 0\}_{apatite}//\{112\}_{garnet}$ and $<11\bar{2}\ 0>_{apatite}//<112>_{garnet}$ have small mismatches and both $\{0001\}_{apatite}//\{111\}_{garnet}$ and $<0001>_{apatite}//<111>_{garnet}$ have small mismatches (Table 1).

5.2 | Rutile

We analysed EBSD data for 96 rutile LAMs with SPO parallel to $<111>_{garnet}$ in the Brimfield Schist samples (Keller & Ague, 2019), 250 rutile LAMs in the Wirtbartl garnet cores (Griffiths et al., 2016) and 184 rutile LAMs, 79% of which have SPO parallel to $<111>_{garnet}$, in the Wirtbartl garnet rims (Griffiths et al., 2020). Rutile results are given in Table 2 and Figure 4. Among the low-index structural elements we considered, rutile can form nine planar alignments and five directional alignments with mismatches ≤1 Å with garnet (Table 2). In total, 12% of rutiles lack one of the analysed alignments. All analysed planar and directional alignments are present in the data. At least one of the planar alignments is present for 85% of the dataset, and at least one of the directional alignments is present for 66% of the dataset. The three smallest planar mismatches (in addition to higher-mismatch alignments) and the five smallest direction mismatches form edge-to-edge matching COR (Figure 4). The most common rutile COR is the edge-to-edge matching COR A^*_{rutile}: $\{100\}_{rutile}//\{110\}_{garnet} +$

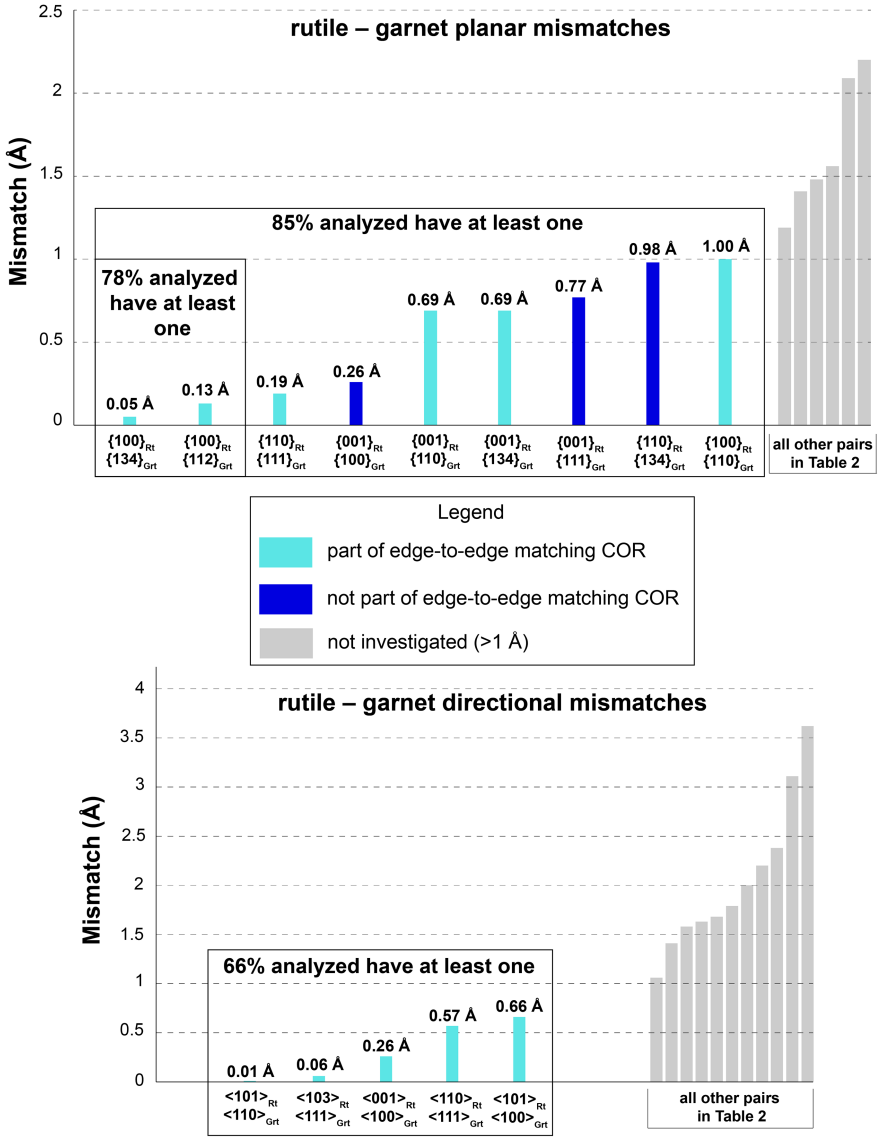

FIGURE 4 Absolute mismatch between low-index structural elements of rutile and garnet (Table 2). In total, 88% of rutiles have at least one of the investigated alignments

$<101>_{rutile}//<100>_{garnet}$ which accounts for 22% of the data (Table 2). This is a result of its widespread prevalence in sample HS00704 in the data of Griffiths et al. (2020) but does not reflect a universal commonality; COR A^*_{rutile} constitutes 1% of the data of Griffiths et al. (2016) and is absent from the data of Keller and Ague (2019). The most common rutile COR that is present in each dataset is the edge-to-edge matching COR A_{rutile}: $\{100\}_{rutile}//\{134\}_{garnet} + <103>_{rutile}//<111>_{garnet}$, which accounts for 13% of the analysed data (Table 2).

5.3 | Ilmenite

We analysed EBSD data for 187 ilmenite LAMs with SPO parallel to $<111>_{garnet}$ in the Brimfield Schist samples (Keller & Ague, 2019) and 100 ilmenite LAMs in the Wirtbartl samples (Griffiths et al., 2016). Ilmenite results are given in Table 3 and Figure 5. Among the low-index structural elements we considered, ilmenite can form nine planar alignments and three directional alignments with mismatches ≤1 Å with garnet (Table 3). Only 2% of the ilmenites lack one of the analysed alignments. All analysed planar and directional alignments are present in the data. At least one of the planar alignments is present for 92% of the dataset, and at least one of the directional alignments is present for 71% of the dataset. The seven lowest-mismatch planar alignments and the three lowest-mismatch directional alignments form edge-to-edge matching COR (Figure 5). The most common ilmenite COR is the edge-to-edge matching COR $A_{ilmenite}$: $\{10\bar{1}\ 0\}_{ilmenite}//\{134\}_{garnet} + <11\bar{2}\ 0>_{ilmenite}//<111>_{garnet}$ (Table 3). This COR accounts for 25% of the analysed data.

5.4 | Corundum

We analysed EBSD data for 180 corundum LAMs in the Wirtbartl samples (Griffiths et al., 2016). Corundum

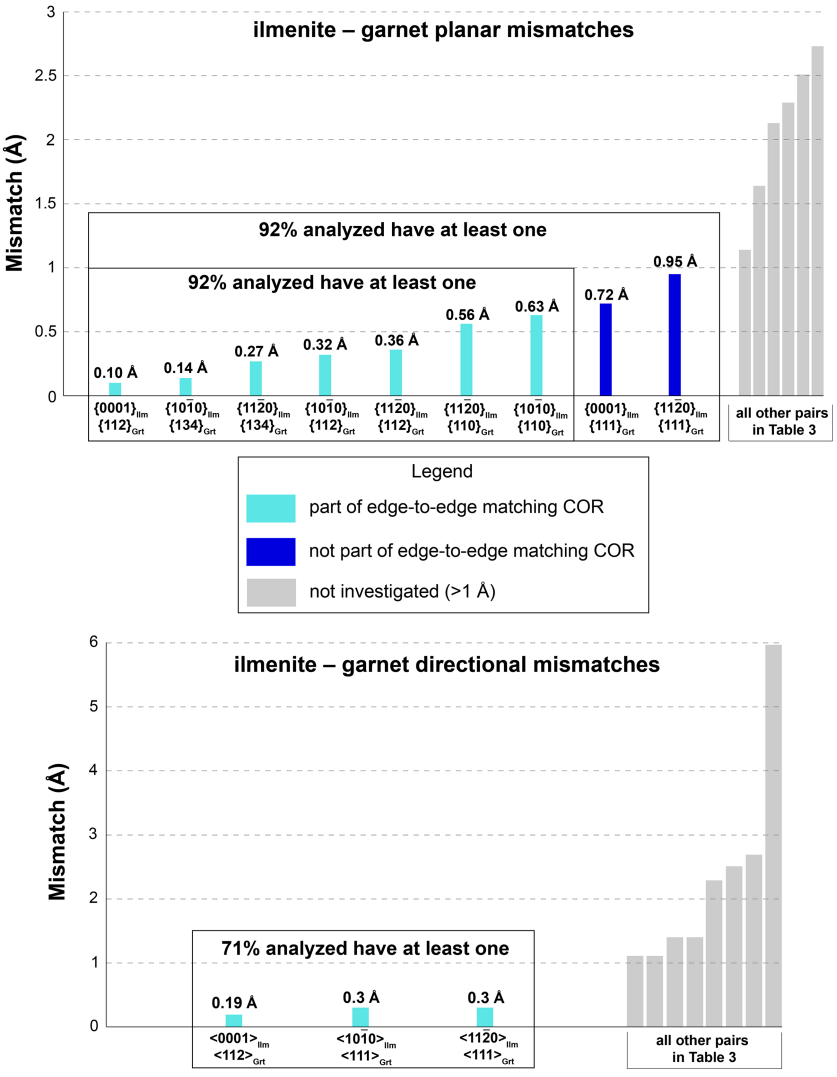

FIGURE 5 Absolute mismatch between low-index structural elements of ilmenite and garnet (Table 3). In total, 98% of ilmenites have at least one of the investigated alignments

results are given in Table 4 and Figure 6. Among the low-index structural elements considered herein, corundum can form nine planar alignments with mismatches ≤1 Å with garnet. Corundum's smallest directional mismatches with garnet are 1.02 Å. The eight lowest-mismatch planar alignments are present in the data. At least one of the planar alignments is present for 95% of the dataset, and one of the two directional alignments is present for 53% of the dataset. The two lowest-mismatch planar alignments (in addition to higher-mismatch alignments) and one of the lowest-mismatch directional alignments form edge-to-edge matching COR (Figure 6). Only 2% of corundums lack one of the analysed alignments. The most common corundum COR is the edge-to-edge matching COR $A_{corundum}$: $\{10\bar{1}\ 0\}_{corundum}//\{110\}_{garnet} + <11\bar{2}\ 0>_{corundum}//<111>_{garnet}$, which accounts for 35% of the dataset (Table 4).

5.5 | Quartz

We analysed EBSD data for 268 quartz LAMs with SPO parallel to $<111>_{garnet}$ in the Brimfield Schist samples (Keller & Ague, 2020). Quartz results are given in Table 5 and Figure 7. Among the low-index structural elements we considered, quartz can form 11 planar alignments and four directional alignments that have mismatches ≤1 Å with garnet. In total, 12% of quartzes lack one of the analysed alignments. All analysed planar and directional alignments are present in the data. At least one of the planar alignments is present for 81% of the dataset, and

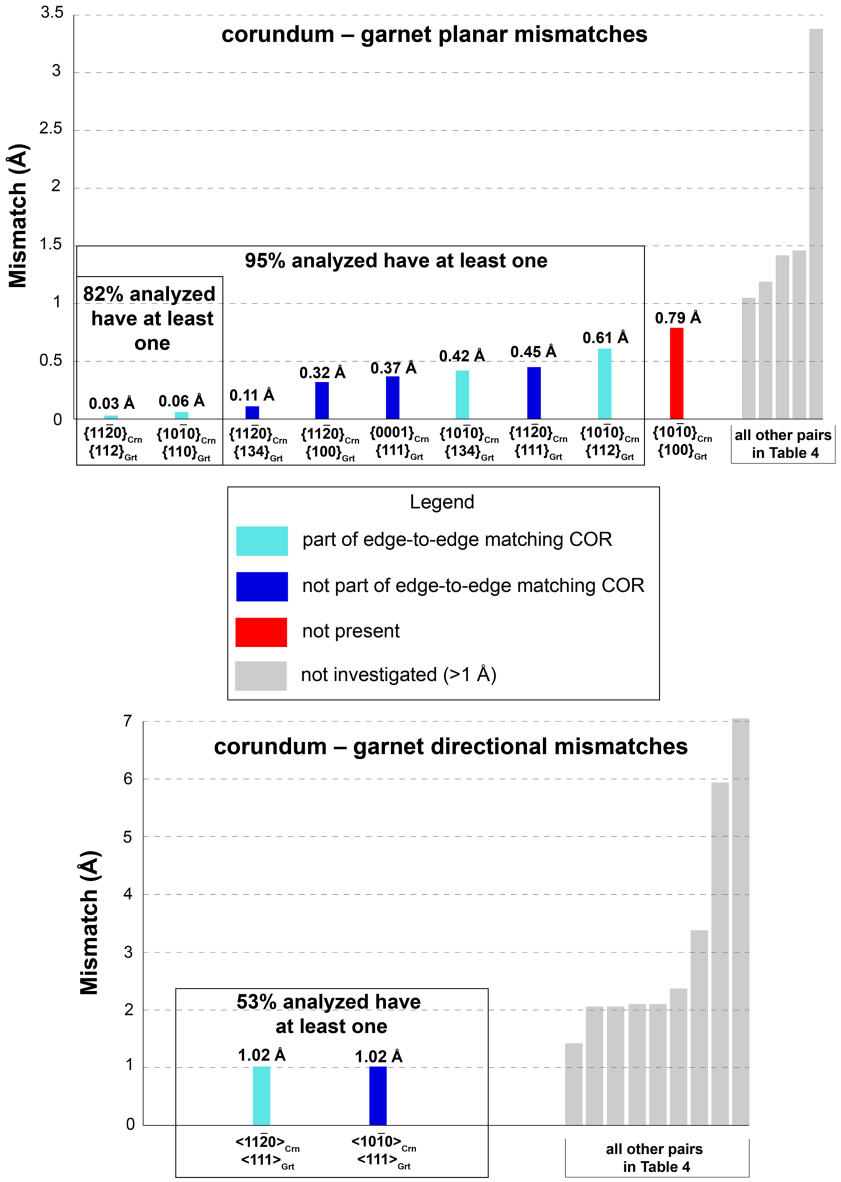

FIGURE 6 Absolute mismatch between low-index structural elements of corundum and garnet (Table 4). In total, 98% of corundums have at least one of the investigated alignments

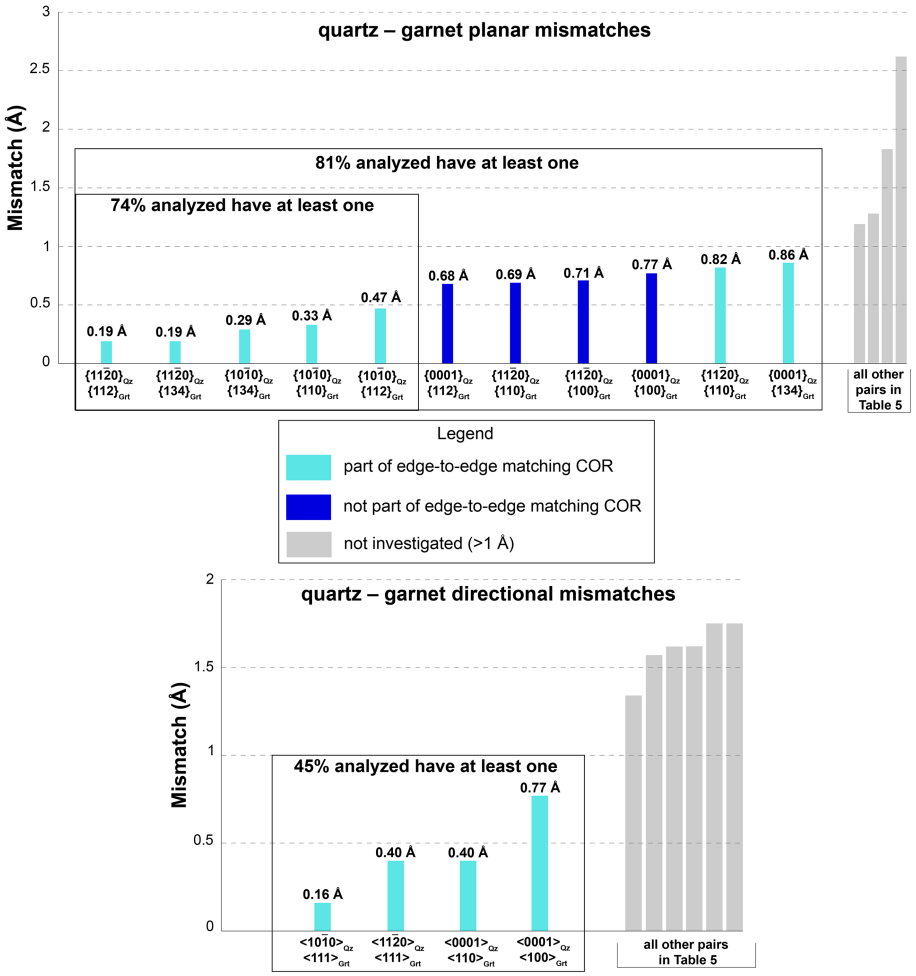

FIGURE 7 Absolute mismatch between low-index structural elements of quartz and garnet (Table 5). In total, 88% of quartzes have at least one of the investigated alignments

at least one of the directional alignments is present for 45% of the dataset. The five lowest-mismatch planar alignments (in addition to higher-mismatch alignments) and the four lowest-mismatch directional alignments form edge-to-edge matching COR (Figure 7). The most common quartz COR is the edge-to-edge matching COR A_{quartz}: $\{10\bar{1}\ 0\}_{quartz}//\{134\}_{garnet} + <11\bar{2}\ 0>_{quartz}//<111>_{garnet}$, which accounts for 12% of the dataset (Table 5).

Although quartz exsolution requires *UHP* precursor majoritic garnet (Keller & Ague, 2020), the *P–T* conditions at which quartz exsolves remain somewhat enigmatic. Calculations in this work used α-quartz–garnet pairs because α-quartz is stable to higher pressures than β-quartz in the temperature range where the two polymorphs co-exist (e.g., Swamy et al., 1994). The same alignments have mismatches ≤1.0 Å for both α-quartz and β-quartz, although the relative magnitudes of some mismatches change. Thus, all alignments tested for α-quartz are applicable to β-quartz. Mismatches were not evaluated for coesite–garnet pairs because no preserved coesite has been found in the Brimfield Schist samples, although quartz LAMs with monoclinic cross sections, inferred to be paramorphs after coesite, are present (Keller & Ague, 2020). Nonetheless, coesite exsolution from garnet has been documented (Alifirova et al., 2015) and may be relevant in cases of quartz exsolution from garnet.

5.6 | Results for all species

Each LAM species investigated forms edge-to-edge matches with garnet, demonstrating that the edge-to-edge matching model has predictive value in garnet systems. Calculations require only mineral unit cell parameters. Between 88% and 98% of LAMs for each species have at least one of the alignments with garnet predicted by mismatch calculations (Tables 1–5). Edge-to-edge matches are recognized in each dataset from each locality. We emphasize that for each mineral, the most common COR fulfils the criteria for edge-to-edge matching and is more common than the 'no COR' category. Each dataset shows a distribution of edge-to-edge

TABLE 6 Morphology versus COR for LAMs in the Brimfield Schist garnets

	No match	1 match	2 or more matches	Edge-to-edge matching
Brimfield Schist needles (all) ($n = 300$)	5%	21%	23%	51%
Brimfield Schist plates (all) ($n = 201$)	12%	23%	24%	41%
Brimfield Schist 'unclear' (all) ($n = 81$)	14%	26%	28%	32%
Brimfield Schist apatite needles ($n = 25$)	0%	8%	8%	84%
Brimfield Schist apatite plates ($n = 3$)	33%	0%	33%	33%
Brimfield Schist apatite 'unclear' ($n = 3$)	33%	0%	67%	0%
Brimfield Schist ilmenite needles ($n = 62$)	5%	18%	13%	65%
Brimfield Schist ilmenite plates ($n = 100$)	1%	15%	26%	58%
Brimfield Schist ilmenite 'unclear' ($n = 25$)	0%	20%	20%	60%
Brimfield Schist quartz needles ($n = 156$)	6%	26%	32%	36%
Brimfield Schist quartz plates ($n = 83$)	20%	30%	23%	27%
Brimfield Schist quartz 'unclear' ($n = 29$)	17%	38%	21%	24%
Brimfield Schist rutile needles ($n = 57$)	5%	18%	14%	65%
Brimfield Schist rutile plates ($n = 15$)	33%	40%	13%	13%
Brimfield Schist rutile 'unclear' ($n = 24$)	21%	21%	42%	17%

Note: All analysed LAMs have SPO parallel to $<111>_{garnet.}$ Rutile, apatite and ilmenite data are from Keller and Ague (2019), and quartz data are from Keller and Ague (2020). Abbreviations: COR, crystallographic orientation relationship; LAM, lamellar to acicular microinclusion.

TABLE 7 Morphology versus COR for rutile LAMs in the Brimfield Schist and Wirtbartl samples

	No match	1 match	2 or more matches	Edge-to-edge matching
Brimfield Schist rutile needles (n = 57)	4%	18%	14%	65%
Brimfield Schist rutile plates ($n = 15$)	33%	40%	13%	13%
Brimfield Schist rutile 'unclear' ($n = 24$)	21%	21%	42%	17%
Wirtbartl rutile needles ($n = 146$)	0%	0%	19%	81%
Wirtbartl rutile 'equant' ($n = 6$)	0%	17%	17%	67%
Wirtbartl rutile 'unclear' ($n = 29$)	7%	24%	17%	52%

Note: Brimfield Schist data are from Keller and Ague (2019), and Wirtbartl data are for garnet rims from Griffiths et al. (2020).
Abbreviations: COR, crystallographic orientation relationship; LAM, lamellar to acicular microinclusion.

matching COR, but no two datasets show the same distribution, suggesting that edge-to-edge matching COR distributions preserve information about each rock's history and in some cases, each individual garnet's history (see Section 6).

5.7 | Morphological connections to COR

We compiled COR data by LAM shape in datasets for which morphological characterizations are available (Griffiths et al., 2020; Keller & Ague, 2019; Keller & Ague, 2020). Results from the Brimfield Schist show that for each mineral (apatite, ilmenite, quartz and rutile), needles are more likely to have edge-to-edge matching COR than other types of COR or no COR than other LAM shapes (Table 6). Needles are also more likely to have edge-to-edge matching COR than equant forms like plates or lamellae, or LAMs with unclear morphologies. The highest fraction of 'no COR' among needles for a LAM mineral is 6% (quartz). Comparison of rutile data between the Brimfield Schist and Wirtbartl samples (Table 7) shows that both localities have the same trends noted above. These findings have implications for the morphologies of precipitates and the effects of edge-to-edge matching COR on precipitate nucleation and growth (see Section 6).

5.8 | Preliminary edge-to-edge matching results for other rutile datasets

Other studies have published analyses of crystallographic data for rutile LAMs in garnet. Some of these studies present analysed and categorized EBSD data without raw data and others present TEM results. We used the information provided in these works to test for the presence of edge-to-edge matching COR and found that in each work, low-mismatch alignments predicted by our method are present. Some of these datasets directly confirm the presence of edge-to-edge matching COR and the rest offer strong evidence that edge-to-edge matching COR are present but require further analysis to test this hypothesis. Because the results of these studies use varied analytical frameworks and COR groupings, results discussed in this section are not presented in the figures or tables herein but are noteworthy as promising preliminary tests that the edge-to-edge matching model is globally applicable to LAMs in garnet. Re-analysis of the original data of these studies will further test the edge-to-edge matching model for precipitates in garnet and will enable hypothesis testing of the factors affecting COR formation (see Section 6).

Proyer et al. (2013) studied rutile needles in garnet from the *UHP* Kimi Complex of Greece. They found that the majority of rutile have $<103>_{rutile}//<111>_{garnet}$, an alignment predicted by our model. Their Figure 2 shows that the edge-to-edge matching COR $\{100\}_{rutile}//\{112\}_{garnet} + <103>_{rutile}//<111>_{garnet}$ (COR B_{rutile} in Table 3) and $\{100\}_{rutile}//\{134\}_{garnet} + <103>_{rutile}//<111>_{garnet}$ (COR A_{rutile} in Table 3), which were not recognized at the time of their work, are present in the Kimi Complex samples, although the relative proportions are unclear. Other edge-to-edge matching COR may also be present.

Xu and Wu (2017) studied rutile COR in garnet from the *UHP* Lüliangshan garnet peridotite. Of the 99 rutile LAMs studied, 78% have $<103>_{rutile}//<111>_{garnet}$, an alignment predicted by our model. A total of 41% of rutile have $<103>_{rutile}//<111>_{garnet} + \{110\}_{rutile}//\{111\}_{garnet}$. Of rutiles in the datasets of Griffiths et al. (2016), Griffiths et al. (2020) and Keller and Ague (2019) with $<103>_{rutile}//<111>_{garnet} + \{110\}_{rutile}//\{111\}_{garnet}$, 98% also have $\{100\}_{rutile}//\{134\}_{garnet}$, which forms edge-to-edge matching COR A_{rutile} (Table 3). We hypothesize that rutiles with $<103>_{rutile}//<111>_{garnet} + \{110\}_{rutile}//\{111\}_{garnet}$ analysed by Xu and Wu (2017) also have $\{100\}_{rutile}//\{134\}_{garnet}$ and achieve edge-to-edge matching, but further analysis is required to test this. In addition, other edge-to-edge matching COR may be present.

Hwang et al. (2016) analysed TEM data of rutile needles in garnet from the *UHP* Sulu Terrane of China and Erzgebirge of Germany, as well as in star garnet from Idaho, USA. Their results confirm the presence of both low-mismatch alignments and edge-to-edge matching COR for each of these localities. Of rutile needles from four-rayed Idaho star garnet ($n = 25$), ~95% have edge-to-edge matching COR A_{rutile} identified in this work (Table 3). Of rutile needles in six-rayed Idaho star garnet ($n = 58$), approximately ≥72% have edge-to-edge matching COR identified in this work: ~28% have COR C_{rutile}, ~16% have COR A_{rutile}, and ~29% have COR B_{rutile} (Table 3). We note that the COR $\{100\}_{rutile}//\{110\}_{garnet} + <001>_{rutile}//<100>_{garnet}$ (COR-5 of Hwang et al., 2016; 19% of six-rayed Idaho star garnet rutile) also appears to fulfil the criteria for edge-to-edge matching, but further analysis is required to confirm this. Of rutile needles in *UHP* eclogite garnet from the Sulu Terrane ($n = 19$), ~63% have the edge-to-edge matching COR identified in this work: ~53% have COR A_{rutile} and ~11% have COR B_{rutile} (Table 3). Of rutile needles in the *UHP* Erzgebirge saidenbachite garnets ($n = 15$), ~67% have the edge-to-edge matching COR identified in this work: ~47% have COR A_{rutile} and ~20% have COR B_{rutile} (Table 3). These TEM data confirm the prevalence of the low-mismatch alignments and edge-to-edge matches we identify for rutile (Table 3) and demonstrate that these COR may be recognized in TEM data.

5.9 | Preliminary edge-to-edge matching results for pyroxene and amphibole

Crystallographic analyses have also been published for pyroxene (Spengler, 2006; Xu & Wu, 2017; Zhang et al., 2011) and amphibole (Song et al., 2005; Xu & Wu, 2017) LAMs in garnet. Original EBSD data are not available from these studies, so a full analysis of edge-to-edge matching was not possible. Nonetheless, preliminary analysis of the published data indicates that low-mismatch alignments dominate the datasets and that edge-to-edge matching is most likely achieved by pyroxene precipitates in garnet.

The COR $\{100\}_{pyroxene}//\{112\}_{garnet} + \{010\}_{pyroxene}//\{110\}_{garnet} + <001>_{pyroxene}//<111>_{garnet}$ is reported for orthopyroxene and clinopyroxene precipitates in garnet from garnet peridotite on the island of Otrøy in Norway (Zhang et al., 2011) and for clinopyroxene precipitates in the Lüliangshan garnet peridotite of the North Qaidam *UHP* terrane (Xu & Wu, 2017). This COR is essentially equivalent to the COR $\{100\}_{clinopyroxene}//\{112\}_{garnet} + \{010\}_{clinopyroxene}//\{110\}_{garnet} + (\bar{1}\ 02)_{clinopyroxene}//\{111\}_{garnet}$ reported by Spengler (2006) for clinopyroxene precipitates from the

same locality because the pole to $(\bar{1}\ 02)_{diopside}$ is <1° from $<001>_{diopside}$ (Hwang et al., 2013).

The alignments $\{100\}_{pyroxene}//\{112\}_{garnet} + <001>_{pyroxene}//<111>_{garnet}$ and $\{010\}_{pyroxene}//\{110\}_{garnet} + <001>_{pyroxene}//<111>_{garnet}$ both fulfil the geometric criterion of edge-to-edge matching for enstatitic orthopyroxene and diopsidic clinopyroxene. Mismatch calculations for garnet compositions between the $Py_{25}Alm_{55}Gro_{20}$ garnet used in this work and the $Py_{87}Alm_{13}$ used by Zhang et al. (2011) show results of a very similar misfit range to the LAM minerals we studied (0.01 to 1.13 Å; Tables S2 and S3). The largest misfit is only ~5%, well within the bounds reported for semi-coherent matches (e.g., Zhang & Kelly, 2005) and may vary given the complex solid solution of pyroxene and garnet and factors such as Fe–Mg exchange and Na substitutions that set unit cell parameters. It appears highly likely that orthopyroxene and clinopyroxene form edge-to-edge matches with garnet, but further work should test this hypothesis using a detailed treatment of the complex solid solutions involved.

Xu and Wu (2017) report COR for exsolved sodic amphibole LAMs in *UHP* garnet from the Lüliangshan garnet peridotite. They report the COR $(010)_{amphibole}//\{112\}_{garnet} + (100)_{amphibole}//\{110\}_{garnet} + <001>_{amphibole}//<111>_{garnet}$ for 21% of the amphiboles and show that an additional 30% of amphiboles have $<001>_{amphibole}//<111>_{garnet}$. In their TEM analysis of amphiboles in the same samples, Song et al. (2005) showed that the length of $<001>_{amphibole} = 9.8–10.0$ Å. Alignment of $<001>_{amphibole}$ (~10 Å) parallel to $<111>_{garnet}$ (~20 Å), is similar to the common rutile alignment $<103>_{rutile}$ (~10 Å) parallel to $<111>_{garnet}$ (~20 Å) that facilitates edge-to-edge matching COR (Figure 2c,d; Table 3). The presence of a low-mismatch direction alignment and a common COR aligning planar and direction elements with the necessary geometries strongly suggest that edge-to-edge matching COR can form between amphibole and garnet. A detailed study analysing the EBSD data of Xu and Wu (2017) and considering the complex solid solution of amphibole could test this hypothesis.

5.10 | COR classification using edge-to-edge matching

Edge-to-edge matching introduces a new way to classify the COR of LAMs in garnet. The high symmetry of garnet and the relatively high symmetry of some LAM minerals (e.g., rutile and apatite) means that if two low-index structural elements are aligned, more structural elements may also be aligned. For example, edge-to-edge matching COR A^*_{rutile} has two elements that form an edge-to-edge match, as well as three planar alignments that do not form an edge-to-edge match with the aligned directions: $\{100\}_{rutile}//\{112\}_{garnet}$, $\{110\}_{rutile}//\{134\}_{garnet}$, and $\{001\}_{rutile}//\{111\}_{garnet}$. All rutiles with edge-to-edge matching COR A^*_{rutile} ($n = 116$) show these same five alignments. This is because if any two alignments are prescribed, both crystal structures have no degrees of freedom and any other matches are also fixed (a 'specific COR'). Thus, any two of these five alignments could be chosen to describe the orientations of the garnet and rutile pair. Because the two alignments that constitute an edge-to-edge match have clear phenomenological meaning, we suggest that COR reporting be standardized to an edge-to-edge match, where present. Otherwise, COR could be classified in terms of the lowest mismatch alignments.

The dominance of low-mismatch alignments in the datasets (Figures 3–7) demonstrates that although the conservative absolute mismatch cut-off we chose provided valuable data, the vast majority of common edge-to-edge matching COR can be classified with the few alignments that have the smallest mismatch for each LAM species. Thus, for common edge-to-edge matching COR, the percentage misfit between the structures that form the edge-to-edge match is likely somewhat less than 10%, a cut-off suggested as generally denoting good fit (Zhang & Kelly, 2005).

6 | DISCUSSION

6.1 | Significance and uses of edge-to-edge matching COR

Consistent development of edge-to-edge matching COR between diverse LAMs and garnet from localities worldwide suggests that edge-to-edge matches represent low-energy, preferred alignments for precipitates as demonstrated in exsolved metallic systems (Easton et al., 2016; Kelly & Zhang, 2006). A variety of edge-to-edge matches or their constituent low-mismatch alignments may form for apatite, rutile, ilmenite, corundum and quartz LAMs in garnet, and edge-to-edge matching also appears likely for pyroxene and amphibole. We conclude that edge-to-edge matches, in addition to chemical and textural evidence (see Section 1), are a clear indicator that these LAMs exsolved from garnet. Despite crystallographic and chemical evidence, some workers take alternative viewpoints, which we address in Section 6.3. As metallurgical work has shown, COR are not always present between structural elements of host and precipitate,

which may form COR relative to an inclusion upon which they nucleate heterogeneously (e.g., Cho et al., 2002) or form COR but lose it during growth (Miao et al., 2015; Nabarro, 1940; Weatherly & Nicholson, 1968). It is thus crucial to note that the absence of a particular COR or widespread lack of COR in a sample does not preclude an exsolution origin. It is also possible that precipitates that show either a planar match or a directional match with the host, but not a full edge-to-edge match, had an edge-to-edge match at very small precipitate size but lost one match as a result of 'breaking away' and realizing an incoherent boundary with the host.

In analysing EBSD data for the presence of edge-to-edge matches, we limited our search from among a large number of possible alignments to those with absolute mismatch ≤1 Å (or in the case of corundum, to the alignment with the smallest mismatch) at a repetition interval of ≤1:5. These limits, like those set in previous studies considering matches between lattices of different materials (e.g., Griffiths et al., 2016), are intended to limit the search to configurations where atoms readily coincide. We found that overwhelmingly, edge-to-edge matches form from alignments with the smallest few mismatches and that repetition intervals of 1:1 to 1:3 constitute the vast majority of the edge-to-edge matches (Tables 1–5; Figures 3–7). This demonstrates that although our search criteria were somewhat more extensive than have been considered in previous work, we nonetheless arrived at the general principle that smaller mismatches at ratios closer to 1:1 tend to be favoured (e.g., Christian, 2002). This suggests that the degree of fit at the host–precipitate interface, in this case represented by regular coincidence of atomic sites that probably facilitates bond sharing, exerts a stabilizing effect upon the exsolved phase.

Results show that the several alignments with the smallest mismatches preferentially form (Figures 3–8). It is not the case, however, that the alignment with the smallest mismatch is always the most common. The rutile directional alignments $<101>_{rutile}//<110>_{garnet}$ (0.01 Å) and $<103>_{rutile}//<111>_{garnet}$ (0.06 Å) are an illustrative example. The alignment $<101>_{rutile}//<110>_{garnet}$ is present for 12% of the data and the alignment $<103>_{rutile}//<111>_{garnet}$ is present for 29% of the data. Edge-to-edge matching COR with $<103>_{rutile}//<111>_{garnet}$ are more than twice as common as edge-to-edge matching COR with $<101>_{rutile}//<110>_{garnet}$ (Table 2). We hypothesize that these differences in occurrence are a result of the inherent geometry of these structures. Namely, $<103>_{rutile}$ is parallel to a greater number of low-index rutile planes with low mismatches to garnet planes than $<101>_{rutile}$ (Table 2). This appears to allow $<103>_{rutile}$ to be part of a greater number of edge-to-edge matches than $<101>_{rutile}$.

Although the vast majority of the analysed precipitates form alignments with garnet characterized by the few smallest mismatches (Figures 3–7), edge-to-edge matches that do not incorporate the single smallest mismatch for each mineral are common in the analysed datasets. This suggests that it is not necessarily the smallest mismatch on one or two interfaces that solely governs reduction of $\Delta G_{surface} + \Delta G_{strain}$, but rather the total energy reduction that the precipitate can achieve, considering the entire surface of the host–precipitate contact. In some cases, an edge-to-edge match with moderately small mismatches can apparently achieve equal or

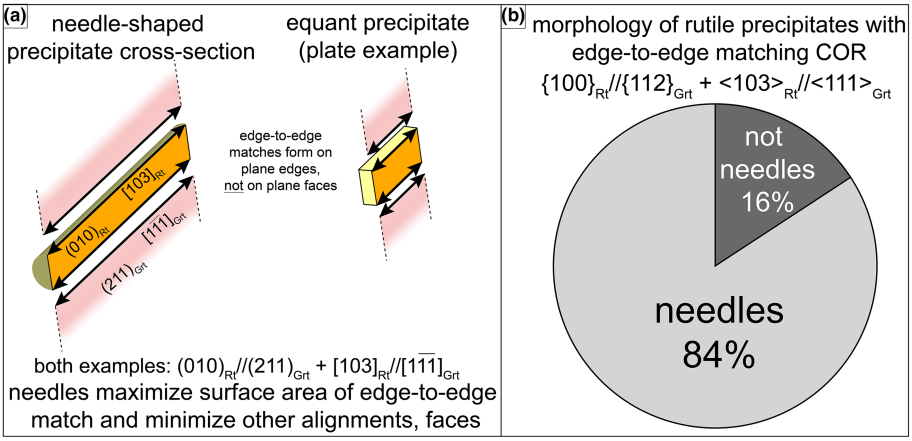

FIGURE 8 Connection between morphology and edge-to-edge matching crystallographic orientation relationship (COR) (Table 6). (a) Sketch of needle- and plate-shaped precipitates illustrating structural elements forming the edge-to-edge matching COR $\{100\}_{rutile}//\{112\}_{garnet} + <103>_{rutile}//<111>_{garnet}$. See Section 4 for COR notation. (b) Fraction of lamellar to acicular microinclusions (LAMs) with the illustrated edge-to-edge matching COR by morphology. Data are from rutile datasets with associated morphological data (Griffiths et al., 2020; Keller & Ague, 2019)

greater energy reduction than a single low-mismatch alignment. Similar behaviour has been observed in controlled exsolution experiments. Hay (2007) found a range of interfacial energies calculated from COR of exsolved Y–Al compounds, and that some observed COR had higher interfacial energies than theoretical COR absent in the sample. This suggests a role for environmental criteria as well as interfacial energies for determining COR. Determination of these criteria is an outstanding challenge in the study of solid-state phase transformations in many crystalline materials (e.g., Hay, 2007; Zhang & Kelly, 2009). As is the case for other materials, we infer that COR of precipitates in garnet may be influenced by factors in addition to mismatch at the phase interface. Further study of the similarities of exsolution processes across different materials would be likely proven useful in unravelling the specific behaviour of each system.

We found that the differences in absolute mismatch between low-mismatch alignments can be quite small. For example, the alignments $\{11\bar{2}\ 0\}_{apatite}//\{112\}_{garnet}$ (0.04 Å) and $\{10\bar{1}\ 0\}_{apatite}//\{110\}_{garnet}$ (0.07 Å) have mismatches that differ by 0.03 Å (Figure 3). Both of these alignments are far more common than the alignment $\{0001\}_{apatite}//\{134\}_{garnet}$ (0.07 Å), which does not form edge-to-edge COR that we could recognize. It also may be the case that an alignment that at 298 K has slightly larger mismatch than another alignment has a slightly smaller mismatch at the temperature of exsolution, for example 700°C. Factors that exert selective pressure for some alignments over others, even when both appear energetically favourable, deserve further inquiry and would prove useful in deciphering the precise meanings of COR distributions. A particularly promising approach could make use of a sample with robustly characterized geologic history to consider how any different populations of COR might represent exsolution at different *P*–*T* conditions.

Multiple possible edge-to-edge matches suggest that although each edge-to-edge match likely lowers $\Delta G_{surface} + \Delta G_{strain}$ and favours precipitate nucleation and growth, a complex interplay of factors connects energetic minima represented by different edge-to-edge matches and COR described by individual low-mismatch alignments. Furthermore, the presence of meaningful low-mismatch alignments and edge-to-edge matches makes the absence of COR for some precipitates worthy of further investigation. More study is necessary to understand the energetic relationships between different COR, but it is nonetheless clear that the distributions of edge-to-edge matches and low-mismatch alignments in a sample must be indicative of environmental factors influencing precipitate growth. As with the development of edge-to-edge matches, metallurgical studies can inform future work on these factors in geological systems. We outline a few examples below of how undercooling, strain or cooling rate might affect edge-to-edge matching COR formation.

Precipitate nucleation upon dislocations can lower the activation energy of nucleation (e.g., Cahn, 1957; Gómez-Ramírez & Pound, 1973; Russell, 1980) and might influence COR development, but does not necessarily prevent COR formation (e.g., Cahn, 1957). Experimental results (e.g., Bailey, 1963; Beaven & Butler, 1980) confirm that dislocations act as precipitate nucleation sites. A strain field exists around both a dislocation and a precipitate with different unit cell parameters than its host. This has led to hypotheses that nucleation of precipitates near or on dislocations will be favoured in orientations that cause the overall reduction of strain, most likely by alignment of high-mismatch, strain-generating structures of host and precipitate in the pre-existing strain field (Russell, 1980).

Both the degree of undercooling (Baumann & Williams, 1985; Beaven & Butler, 1980) and the elastic constants of the precipitate (Gómez-Ramírez & Pound, 1973) affect the activation energy of nucleation upon dislocations. In Fe–N alloys, for example, small degrees of undercooling favour heterogeneous precipitate nucleation on edge dislocations, but at larger degrees of undercooling where a greater thermodynamic driving force for precipitation exists, precipitates nucleate equally on any dislocation type (Beaven & Butler, 1980). Somewhat similarly, Al–Li alloys show homogeneous nucleation behaviour at large degrees of undercooling, while smaller degrees of undercooling cause preferential exsolution next to dislocations (Baumann & Williams, 1985). Observations such as these introduce the exciting possibility that different exsolving minerals respond differently to the same environment within the host garnet and therefore may preserve partially overlapping or unique information. If certain COR can be linked to nucleation upon dislocations, these relationships could be used as a proxy for dislocation density in garnet at the time of exsolution, the degree of undercooling (tectonic setting of exsolution), or the relative order of exsolving precipitates. We note that the primary direction along which dislocations form in garnet is $<111>_{garnet}$ (Karato et al., 1995), which is also the close-packed direction in the body-centred cubic garnet structure (Andersson & O'Keeffe, 1977). Favourable direction matches and edge-to-edge matching COR involving $<111>_{garnet}$ (Tables 1–5) combined with nucleation upon dislocations together may contribute to the commonly-observed LAM precipitate SPO parallel to $<111>_{garnet}$.

Some edge-to-edge matching COR may be strain indicators. For instance, edge-to-edge matching COR A^*_{rutile}

is dominant (65%; $n_{total} = 165$) for rutile LAMs in the garnet rim of sample HS00704 of Griffiths et al. (2020), but extremely rare (3%; $n_{total} = 269$) for rutile LAMs in garnets from sample 04T26K, which was collected from a different lens of the same rock type 2 km away (Griffiths et al., 2016; Griffiths et al., 2020). Rocks in this unit were strongly deformed during eclogite facies metamorphism, the effects of which have been noted on their garnet microstructures (Bestmann et al., 2008; Griffiths et al., 2014). Edge-to-edge matching COR A^*_{rutile} has both the highest rutile-garnet planar and direction mismatches considered in this study. It is possible that this COR preferentially forms in garnets that preserved large amounts of strain at the time of exsolution and is favoured by deformation structures in garnet. Edge-to-edge matching COR A^*_{rutile} is absent from the Brimfield Schist garnets ($n_{total} = 96$) (Keller & Ague, 2019), which reached peak temperatures >1000°C, several hundred°C higher than estimates of the Wirtbartl garnets (Griffiths et al., 2020); these extreme temperatures likely annealed prograde strain. These trends are an example of how COR might be developed as indicators of the physical state of the host rock at the time of exsolution.

Cooling rate demonstrably affects precipitate morphology and which phases form as precipitates in alloy systems (e.g., Shewmon, 1969). Therefore, certain COR may be favoured by the effects of cooling rate on nucleation behaviour, and by extension, $\Delta G_{surface}$. Analyses of diffusional relaxation of precipitate-forming component depletion halos around LAMs in host garnet (Ague & Eckert, 2012; Axler & Ague, 2015) would be a powerful and internally consistent tool for quantitatively linking COR and cooling rate. Future experimental work may also test the cooling rate hypothesis if exsolved precipitates can be produced in garnet in a laboratory setting.

Evidence suggests that environmental factors such as temperature, strain, cooling rate, degree of undercooling or dislocation density of the host mineral likely affect COR development between precipitates and garnet. Other effects, such as from pressure, also deserve investigation. In the case of silicate exsolutions with extensive solid solution that may affect unit cell parameters, such as pyroxene and amphibole, precipitate chemistry and cation exchange between the exsolved phase and host garnet may also play a role in COR development. Even in cases where, for example, TEM imaging might show that the garnet and precipitate lattices are not coherent in the final preserved texture, the presence of an edge-to-edge matching COR would suggest that an energetically favourable relationship was present during precipitate nucleation and/or early growth and may have facilitated coherency or semi-coherency for the small exsolved nucleus. Loss of coherency during precipitate coarsening is well-documented (Miao et al., 2015; Nabarro, 1940; Weatherly & Nicholson, 1968) and does not preclude interpretation of preserved COR.

6.2 | Edge-to-edge matching and precipitate morphology

Regardless of species, needle-shaped precipitates preferentially have edge-to-edge matching COR rather than other types of COR or no COR (Tables 6 and 7). Of the edge-to-edge matching COR noted in this study, 80% involve a match along $<111>_{garnet}$, the primary LAM SPO direction (Tables 1–5). This suggests that an edge-to-edge match along the length of a needle stabilizes this precipitate shape by maximizing the surface area of the favourable match relative to less favourable matches on other faces (Figure 8). In a similar manner, oxide needles preferentially elongated along directions of similar oxygen packing, and crystallographic plane spacing to host plagioclase have been noted (Ageeva et al., 2020). These characteristics are taken as evidence of an exsolution origin (Bian et al., 2021). Experimental studies of exsolution induced in laboratory settings have shown coherent structural matches parallel to long axes of lath- or needle-shaped precipitates (e.g., Bailey, 1963; Phillips et al., 1980a; Weatherly & Nicholson, 1968; Winkelman et al., 2007). Needle- and plate-shaped precipitates also produce less total strain within the host matrix than spherical morphologies (Nabarro, 1940). These stabilizing effects can largely explain why exsolved LAMs have such markedly different shapes than overgrown, more equant inclusions in garnet, particularly those that have recrystallized at high temperature (Cesare et al., 2021).

We hypothesize that needle-shaped LAMs with edge-to-edge matches along $<111>_{garnet}$ may nucleate by forming that edge-to-edge match and grow along it. Coherent matching along needle length could explain the atypical elongation of various species such as rutile, ilmenite and quartz parallel to crystal axes other than the *c*-axis. Free-standing crystals of these minerals rarely, if ever, show these characteristics, which strongly suggest that stabilizing, low-energy matches guide needle growth, as would be expected for a precipitate surrounded by a solid host. We also hypothesize that single low-mismatch alignments (e.g., only a direction or planar match) along the needle length could stabilize this precipitate shape, although likely not as efficiently as an edge-to-edge match. We further note that coherency arguments have also been made for plate-shaped precipitates (e.g., Howe et al., 1985; Nabarro, 1940) and are likely relevant to exsolution in garnet. Stabilization of plates requires

further detailed study because the dominant faces of plates extend in several directions. It is thought, however, that in order to readily accommodate elastic strain, plate-shaped precipitates tend to form with their wide faces perpendicular to the direction of maximum compressibility in the host (e.g., Baumann & Williams, 1985).

There has been prior geological study of the dependence of habit planes, the interfaces separating host and precipitate, on temperature (e.g., Fleet et al., 1980; Robinson et al., 1977). This is a related, but distinct question from the COR of a precipitate. Future work focusing on relationships between edge-to-edge matching and habit planes in garnet-precipitate systems would provide insight into exsolution mechanisms and may provide new ways to retrieve petrological information from garnet exsolution textures.

6.3 | Edge-to-edge matching COR and non-exsolution hypotheses

For some LAM minerals, such as rutile, the presence of a variety of COR and the apparent unsuitability of closed-system precipitation reactions have led to hypotheses that LAMs in garnet form by co-growth of LAM minerals with garnet (Griffiths et al., 2020; Hwang et al., 2016; Wang et al., 1999) or fluid-mediated replacement reactions (Hwang et al., 2019), rather than by exsolution. We briefly address below how these alternative hypotheses are not necessary to explain the observed features in garnet considered herein. We also lay out some ways in which future work can further test LAM formation hypotheses; additional discussion of these hypotheses can be found in, for example, Proyer et al. (2013) and Keller and Ague (2019).

Diverse COR do not preclude an exsolution origin for LAMs because unequivocal exsolution systems such as anthropogenic alloys in tightly controlled laboratory settings and natural meteorites may form precipitates with a variety of COR, or no COR, within the same sample (e.g., Bunge et al., 2003; Cayron, 2014; Cho et al., 2002; Guo et al., 2004; He et al., 2006; Kelly & Zhang, 2006; Lambert-Perlade et al., 2004; Lin et al., 1979; Miao et al., 2015; Nolze et al., 2005; Winkelman et al., 2007; Zhang & Kelly, 1998; Zhong et al., 2011). Various factors relevant to geological systems have been hypothesized to cause COR variations in metallic systems, including exsolution over a temperature range (He et al., 2006) or amount of precipitate coarsening (Miao et al., 2015). The edge-to-edge matching hypothesis offers a testable framework to explain why the same garnet might have precipitates with several different COR. For example, one precipitate population may have grown at higher temperature and one at lower temperature or one during a low-strain period and one during a high-strain period. Edge-to-edge matching theory also explains why COR with small mismatches dominate datasets for each LAM mineral (Tables 1–5; Figures 3–7).

The edge-to-edge matching COR we find commonly involve $<111>_{garnet}$, the close-packed direction in garnet (Andersson & O'Keeffe, 1977). Edge-to-edge matches often involve close-packed directions (Kelly & Zhang, 2006; Zhong et al., 2011), likely because alignment of close-packed directions between host and precipitate produces a low-energy configuration (Shiflet & van der Merwe, 1994). The exsolution hypotheses explain the common orientation of LAMs along $<111>_{garnet}$ through a combination of several factors. Garnet octahedral sites, in which key precipitate-forming ions substitute (e.g., Ti^{4+}), lie along $<111>_{garnet}$. This vector is also the primary direction along which dislocations form in garnet (Karato et al., 1995). Although precipitate nucleation mechanisms deserve much further investigation, if dislocations are favourable precipitate nucleation sites, then a plausible path of least resistance for precipitate growth is attachment of components, released from solid solution in garnet, together upon dislocations along $<111>_{garnet}$.

A successful test of the co-growth hypothesis to explain LAM orientation along $<111>_{garnet}$ would have to show that the faces upon which LAM nucleation is inferred were present during garnet growth and, furthermore, would have to explain why LAM growth followed $<111>_{garnet}$. Testing of the replacement hypothesis should explain how replacement fronts propagating through LAM-free garnet would deposit LAM along garnet axes (e.g., $<111>_{garnet}$). This behaviour would directly contradict the observed patterns in replacement reactions that involve an advancing planar front of porosity (Ague & Axler, 2016; Pearce & Escolme, 2021; Putnis & John, 2010; Putnis & Putnis, 2007) or a reaction rim (e.g., Keller & Ague, 2018).

Other textural hurdles to deposition and co-growth should also be addressed if these hypotheses are invoked. For both hypotheses, LAM phases must be shown, such as by equilibrium phase diagram modelling or experimental petrology, to be stable at the conditions envisioned for LAM growth in the rock matrix or from an infiltrating fluid. Furthermore, an argument for co-growth should address why, if LAM minerals are nucleating at garnet faces, garnet and LAM species growth rates are precisely matched so that the inclusions do not grow into more irregular forms. Overgrown, rounded inclusions are common in garnet porphyroblasts in rocks of diverse metamorphic grade—why do supposedly co-grown inclusions not have these same shapes as well? In the case of hypothesized co-growth of garnet and rutile, a

lack of geniculated ('knee-twinned') rutile should be addressed, as this habit is common for rutile growing in rock matrices.

In summary, models for the formation of LAMs via oriented attachment of the mineral to a garnet face or formation of LAMs by replacement reactions must overcome the apparent crystallographic, petrologic and textural challenges outlined above, all of which are testable with further study.

Some work has concluded that LAM minerals such as rutile cannot form by exsolution because closed-system exsolution reactions from garnet are difficult to envision (e.g., Wang et al., 1999). The hypothesis of open-system precipitation—the exchange of ions in and out of the garnet system during exsolution (Proyer et al., 2013)—addresses this apparent paradox, and evidence for open-system precipitation has been found in LAM-bearing garnet. For example, in *UHP* garnet from the Erzgebirge (Germany), depletion halos of Ti, P and Na around rutile and apatite precipitates, but the lack of an exsolved Na phase, indicates that open-system precipitation took place and that Na was part of a coupled substitution with Ti and/or P in the precursor *UHP* garnet (Ague & Axler, 2016; Axler & Ague, 2015). Analysis of preserved garnet and precipitate chemistry from *UHP* gneiss of the Central Maine Terrane (USA) shows that loss of Na and gain of Mg and Al following majoritic garnet substitution vectors during open-system precipitation results in balanced garnet chemical formulae (Keller & Ague, 2020). Open-system precipitation of oxide exsolutions from plagioclase is supported by chemical and crystallographic data (Bian et al., 2021). Moreover, open-system behaviour has been demonstrated unequivocally in sulphide systems during solid-state exsolution (Adegoke et al., 2021).

7 | CONCLUSIONS

Edge-to-edge matching COR offer several benefits for the study of exsolution in garnet, and possibly in other mineral systems as well. The crystallography of any exsolved phase can be analysed in the context of edge-to-edge matching, allowing for a unified framework for classifying and comparing LAM datasets. This would greatly expedite efforts to compare COR from different localities and enhances possibilities for comparing the behaviour of different LAM minerals from the same locality. The widespread prevalence, phenomenological significance and comparative prospects of edge-to-edge matching COR make them a valuable tool for gathering information about both exsolved phases and their host garnets at the time of exsolution.

Distributions of edge-to-edge matching COR may be tested as petrogenetic and tectonic indicators in a wide variety of igneous and high-*P*/*T* metamorphic rocks containing exsolved LAMs in garnet. Precipitates in garnet in *UHT* rocks (e.g., Das et al., 2013; Liu et al., 2010; Shinevar et al., 2021), high-pressure granulites (e.g., Keller & Ague, 2018; Marsh & Kelly, 2017), eclogites (e.g., Aulbach, 2020; Ye et al., 2000), *UHP* rocks (e.g., Axler & Ague, 2015; Mposkos & Kostopoulos, 2001), mantle xenoliths (e.g., Alifirova et al., 2015; Haggerty & Sautter, 1990; Sakamaki et al., 2016) and crustal xenoliths (e.g., Ducea et al., 2020; Farmer et al., 2005) together offer an extensive network of diverse formation environments in which to test hypotheses of factors affecting edge-to-edge matching COR formation. If some edge-to-edge matching COR form only, for example, during exsolution at high temperatures, or in highly strained samples, such indicators would prove valuable additions to the analytical techniques used to interrogate extreme metamorphism and processes in the deep lithosphere and asthenosphere.

Edge-to-edge matching COR also show great promise for testing the origin of inclusions suspected to be exsolved from garnet. Generation of precipitates from garnet in laboratory experiments would open exciting avenues for correlation of different edge-to-edge matching COR with formation conditions and precise diagnosis of the physical state of garnet during exsolution, which may otherwise be inaccessible in many samples. This information could be paired with micro-sampled garnet geochronology (e.g., Pollington & Baxter, 2010) to place the information gained from analysis of edge-to-edge matching COR in a temporal context. Edge-to-edge matching may also prove useful for studying exsolution in other geological systems, such as feldspars and pyroxenes, for which it may reflect similar information as is preserved in garnet-precipitate systems.

ACKNOWLEDGEMENTS

This work was supported by the US National Science Foundation Directorate of Geosciences (EAR-0744154, EAR-1250269 and EAR-1753553) and Yale University. We thank J.A. Axler, D.A.D. Evans, A.A. Haws and E.M. Stewart for discussions and R. Abart and A. Proyer for their thorough review comments.

CONFLICT OF INTEREST

The authors declare no conflicts of interest.

DATA AVAILABILITY STATEMENT

The data underlying this article will be shared on reasonable request to the corresponding author. Data from Griffiths et al. (2016) are available online (http://www.

minsocam.org/MSA/AmMin/TOC/2016/Mar2016_data/AM-16-35442.zip). Data from Griffiths et al. (2020) are available online (http://earth.geology.yale.edu/%7eajs/SupplementaryData/2020/Griffiths).

ORCID

Duncan S. Keller https://orcid.org/0000-0002-8369-4399

REFERENCES

Abart, R., Petrishcheva, E., Wirth, R., & Rhede, D. (2009). Exsolution by spinodal decomposition II: Perthite formation during slow cooling of anatexites from Ngoronghoro, Tanzania. *American Journal of Science*, *309*, 450–475. https://doi.org/10.2475/06.2009.02

Adegoke, I. A., Xia, F., Deditius, A. P., Pearce, M. A., Roberts, M. P., & Brugger, J. (2021). A new mode of mineral replacement reactions involving the synergy between fluid-induced solid-state diffusion and dissolution-reprecipitation: A case study of the replacement of bornite by copper sulfides. *Geochimica et Cosmochimica Acta*, in press. https://doi.org/10.1016/j.gca.2021.04.017

Ageeva, O., Bian, G., Habler, G., Pertsev, A., & Abart, R. (2020). Crystallographic and shape orientations of magnetite micro-inclusions in plagioclase. *Contributions to Mineralogy and Petrology*, *175*, 95. https://doi.org/10.1007/s00410-020-01735-8

Ague, J. J., & Axler, J. A. (2016). Interface coupled dissolution-reprecipitation in garnet from subducted granulites and ultrahigh-pressure rocks revealed by phosphorous, sodium, and titanium zonation. *American Mineralogist*, *101*, 1696–1699. https://doi.org/10.2138/am-2016-5707

Ague, J. J., & Eckert, J. O. Jr. (2012). Precipitation of rutile and ilmenite needles in garnet: Implications for extreme metamorphic conditions in the Acadian Orogen, U.S.A. *American Mineralogist*, *97*, 840–855. https://doi.org/10.2138/am.2012.4015

Ague, J. J., Eckert, J. O. Jr., Chu, X., Baxter, E. F., & Chamberlain, C. P. (2013). Discovery of ultrahigh-temperature metamorphism in the Acadian orogen, Connecticut, USA. *Geology*, *41*, 271–274. https://doi.org/10.1130/G33752.1

Alifirova, T. A., Pokhilenko, L. N., & Korsakov, A. V. (2015). Apatite, SiO_2, rutile and orthopyroxene precipitates in minerals of eclogite xenoliths from Yakutian kimberlites, Russia. *Lithos*, *226*, 31–49. https://doi.org/10.1016/j.lithos.2015.01.020

Andersson, S., & O'Keeffe, M. (1977). Body-centered cubic cylinder packing and the garnet structure. *Nature*, *267*, 605–606. https://doi.org/10.1038/267605b0

Aulbach, S. (2020). Temperature-dependent rutile solubility in garnet and clinopyroxene from mantle eclogite: Implications for continental crust formation and V-based oxybarometry. *Journal of Petrology*, *egaa065*, 1–26.

Axler, J. A., & Ague, J. J. (2015). Exsolution of rutile or apatite precipitates surrounding ruptured inclusions in garnet from UHT and UHP rocks. *Journal of Metamorphic Geology*, *33*, 829–848. https://doi.org/10.1111/jmg.12145

Bachmann, F., Hielscher, R., & Schaeben, H. (2010). Texture analysis with MTEX—Free and Open Source Software Toolbox. *Solid State Phenomena*, *160*, 63–68. https://doi.org/10.4028/www.scientific.net/SSP.160.63

Bailey, J. E. (1963). Electron microscope observations on the precipitation of zirconium hydride in zirconium. *Acta Metallurgica*, *11*, 267–280. https://doi.org/10.1016/0001-6160(63)90182-2

Baumann, S. F., & Williams, D. B. (1985). Experimental observations on the nucleation and growth of δ' (Al_3Li) in dilute Al-Li alloys. *Metallurgical Transactions a*, *16*, 1203–1211. https://doi.org/10.1007/BF02670325

Beaven, P. A., & Butler, E. P. (1980). Precipitate nucleation on dislocations in Fe-N. *Acta Metallurgica*, *28*, 1349–1359. https://doi.org/10.1016/0001-6160(80)90004-8

Bestmann, M., Habler, G., Heidelbach, F., & Thöni, M. (2008). Dynamic recrystallization of garnet and related diffusion processes. *Journal of Structural Geology*, *30*, 777–790. https://doi.org/10.1016/j.jsg.2008.02.007

Bian, G., Ageeva, O., Rečnik, A., Habler, G., & Abart, R. (2021). Formation pathways of oriented magnetite micro-inclusions in plagioclase from oceanic gabbro. *Contributions to Mineralogy and Petrology*, *176*, 104. https://doi.org/10.1007/s00410-021-01864-8

Brunet, F., Allan, D. R., Redfern, S. A. T., Angel, R. J., Miletich, R., Reichmann, H. J., Sergent, J., & Hanfland, M. (1999). Compressibility and thermal expansivity of synthetic apatites, $Ca_5(PO_4)_3X$ with W = OH, F and cl. *European Journal of Mineralogy*, *11*, 1023–1036. https://doi.org/10.1127/ejm/11/6/1023

Bunge, J. H., Weiss, W., Klein, H., Wcislak, L., Garbe, U., & Schneider, J. R. (2003). Orientation relationship of Widmanstätten plates in an iron meteorite measured with high-energy synchrotron radiation. *Journal of Applied Crystallography*, *36*, 137–140. https://doi.org/10.1107/S0021889802021386

Cahn, J. W. (1957). Nucleation on dislocations. *Acta Metallurgica*, *5*, 169–172. https://doi.org/10.1016/0001-6160(57)90021-4

Cahn, J. W., Pan, J. D., & Balluffi, R. W. (1979). Diffusion induced grain boundary migration. *Scripta Metallurgica*, *13*, 503–509. https://doi.org/10.1016/0036-9748(79)90078-4

Cayron, C. (2014). EBSD imaging of orientation relationships and variant groupings in different martensitic alloys and Widmanstätten iron meteorites. *Materials Characterization*, *94*, 93–110. https://doi.org/10.1016/j.matchar.2014.05.015

Cesare, B., Parisatto, M., Mancini, L., Peruzzo, L., Franceschi, M., Tacchetto, T., Reddy, S., Spiess, R., Nestola, F., & Marone, F. (2021). Mineral inclusions are not immutable: Evidence of post-entrapment thermally-induced shape change of quartz in garnet. *Earth and Planetary Science Letters*, *555*, 116708. https://doi.org/10.1016/j.epsl.2020.116708

Chawla, K. K., Esmaeili, A. H., Datye, A. K., & Vasudevan, A. K. (1991). Effect of homogeneous/heterogeneous precipitation on aging behavior of SiC_p/Al 2014 composite. *Scripta Metallurgica et Materialia*, *25*, 1315–1319. https://doi.org/10.1016/0956-716X(91)90407-R

Cho, J.-Y., Suh, D.-W., Kang, J.-H., & Lee, H.-C. (2002). Orientation distribution of proeutectoid ferrite nucleated at prior austentite grain boundaries in vanadium-added steel. *ISIJ International*, *42*, 1321–1323. https://doi.org/10.2355/isijinternational.42.1321

Christian, J. W. (2002). *The theory of transformations in metals and alloys* (3rd ed.). Pergamon.

Dahmen, U. (1982). Orientation relationships in precipitate systems. *Acta Metallurgica*, *30*, 63–73. https://doi.org/10.1016/0001-6160(82)90045-1

Dahmen, U., & Westmacott, K. H. (1983). Ledge structure and the mechanism of θ' precipitate growth in Al-cu. *Physica Status Solidi (a)*, *80*, 249–262. https://doi.org/10.1002/pssa.2210800128

Das, K., Tomioka, N., Bose, S., & Ando, J.-I. (2013). On oriented ilmenite needles in garnet porphyroblasts from deep crustal granulites: Implications for fluid evolution and cooling history. *Lithos*, *156–159*, 230–240.

Ducea, M. N., Chapman, A. D., Bowman, E., & Triantafyllou, A. (2020). Arclogites and their role in continental evolution: Part 1: Background, locations, petrography, geochemistry, chronology, and thermobarometry. *Earth-Science Reviews*, *214*, 103375.

Easton, M. A., Qian, M., Prasad, A., & StJohn, D. H. (2016). Recent advances in grain refinement of light metals and alloys. *Current Opinion in Solid State and Materials Science*, *20*, 13–24. https://doi.org/10.1016/j.cossms.2015.10.001

Farmer, G. L., Bowring, S. A., Williams, M. L., Christensen, N. I., Matzel, J. P., & Stevens, L. (2005). Contrasting lower crustal evolution across an archean-proterozoic suture: Physical, chemical and geochronologic studies of lower crustal xenoliths in Southern Wyoming and Northern Colorado. In K. E. Karlstrom & G. R. Keller (Eds.), *The Rocky Mountain Region—An evolving lithosphere: Tectonics, Geochemistry, and Geophysics, American Geophysical Union Geophysical Monograph Series* (Vol. 154, pp. 139–162). American Geophysical Union. https://doi.org/10.1029/154GM11

Fiquet, G., Richet, P., & Montagnac, G. (1999). High-temperature thermal expansion of lime, periclase, corundum and spinel. *Physics and Chemistry of Minerals*, *27*, 103–111. https://doi.org/10.1007/s002690050246

Fleet, M. E., Bilcox, G. A., & Barnett, R. L. (1980). Oriented magnetite inclusions in pyroxenes from the Grenville Province. *Canadian Mineralogist*, *18*, 89–99.

Gibbs, J. W. (1878). On the equilibrium of heterogeneous substances. *Connecticut Academy of Arts and Sciences Transactions*, *3*, 343–524. https://doi.org/10.2475/ajs.s3-16.96.441

Gómez-Ramírez, R., & Pound, G. M. (1973). Nucleation of a second phase along dislocations. *Metallurgical Transactions*, *4*, 1563–1570.

Griffin, W. L., Jensen, B. B., & Misra, S. N. (1971). Anomalously elongated rutile in eclogite-facies pyroxene and garnet. *Norsk Geologisk Tidsskrift*, *51*, 177–185.

Griffiths, T. A., Habler, G., & Abart, R. (2016). Crystallographic orientation relationships in host–inclusion systems: New insights from large EBSD data sets. *American Mineralogist*, *101*, 690–705. https://doi.org/10.2138/am-2016-5442

Griffiths, T. A., Habler, G., & Abart, R. (2020). Determining the origin of inclusions in garnet: Challenges and new diagnostic criteria. *American Journal of Science*, *320*, 753–789. https://doi.org/10.2475/11.2020.01

Griffiths, T. A., Habler, G., Rhede, D., Wirth, R., Ram, F., & Abart, R. (2014). Localization of submicron inclusion re-equilibration at healed fractures in host garnet. *Contributions to Mineralogy and Petrology*, *168*, 1077. https://doi.org/10.1007/s00410-014-1077-4

Guo, Z., Lee, C. S., & Morris, J. W. Jr. (2004). On coherent transformations in steel. *Acta Materialia*, *52*, 5511–5518. https://doi.org/10.1016/j.actamat.2004.08.011

Habler, G., & Griffiths, T. (2017). Crystallographic orientation relationships. In W. Heinrich & R. Abart (Eds.), *Mineral reaction kinetics: Microstructures, textures, chemical and isotopic signatures* (Vol. 16) (pp. 541–585). European Mineralogical Union Notes in Mineralogy.

Haggerty, S. E., & Sautter, V. (1990). Ultradeep (greater than 300 kilometers), ultramafic upper mantle xenoliths. *Science*, *248*, 993–996. https://doi.org/10.1126/science.248.4958.993

Hay, R. S. (2007). Orientation relationships between complex low symmetry oxides: Geometric criteria and interface structure for yttrium aluminate eutectics. *Acta Materialia*, *55*, 991–1007. https://doi.org/10.1016/j.actamat.2006.09.029

He, Y., Godet, S., Jacques, P. J., & Jonas, J. J. (2006). Crystallographic relations between face- and body-centered cubic crystals formed under near-equilibrium conditions: Observations from the Gibeon meteorite. *Acta Materialia*, *54*, 1323–1334. https://doi.org/10.1016/j.actamat.2005.11.008

Hielscher, R., Schaeben, H., & Siemes, H. (2010). Orientation distribution within a single hematite crystal. *Mathematic Geoscience*, *42*, 359–375. https://doi.org/10.1007/s11004-010-9271-z

Howe, J. M. (1997). *Interfaces in materials: Atomic structure, thermodynamics and kinetics of solid-vapor, solid-liquid, and solid-solid interfaces* (1st ed.). Wiley-Interscience.

Howe, J. M., Aaronson, H. I., & Gronsky, R. (1985). Atomic mechanisms of precipitate growth in the Al-Ag system—I. Conventional transmission electron microscopy. *Acta Metallurgica*, *33*, 639–648. https://doi.org/10.1016/0001-6160(85)90027-6

Hwang, S. L., Shen, P., Chu, H. T., Yui, F., & Iizuka, Y. (2013). A TEM study of the oriented orthopyroxene and forsterite inclusions in garnet from Otrøy garnet peridotite, WGR, Norway: New insights on crystallographic characteristics and growth energetics of exsolved pyroxene in relict majoritic garnet. *Journal of Metamorphic Geology*, *31*, 113–130. https://doi.org/10.1111/jmg.12002

Hwang, S.-L., Shen, P., Chu, H. T., & Yui, T. F. (2016). On the forbidden and the optimum crystallographic variant of rutile in garnet. *Journal of Applied Crystallography*, *49*, 1922–1940. https://doi.org/10.1107/S1600576716014151

Hwang, S.-L., Shen, P., Chu, H. T., Yui, T.-F., Iizuka, Y., & Schertl, H.-P. (2019). Rutile inclusions in garnet from a dissolution-reprecipitation mechanism. *Journal of Metamorphic Geology*, *37*, 1079–1098. https://doi.org/10.1111/jmg.12502

Karato, S.-I., Wang, Z., Liu, B., & Fujino, K. (1995). Plastic deformation of garnets: Systematics and implications for the rheology of the mantle transition zone. *Earth and Planetary Science Letters*, *130*, 13–30. https://doi.org/10.1016/0012-821X(94)00255-W

Keller, D. S., & Ague, J. J. (2018). High-pressure granulite facies metamorphism (∼1.8 GPa) revealed in silica-undersaturated garnet-spinel-corundum gneiss, Central Maine terrane, Connecticut, U.S.A. *American Mineralogist*, *103*, 1851–1868.

Keller, D. S., & Ague, J. J. (2019). Crystallographic and textural evidence for precipitation of rutile, ilmenite, corundum, and apatite lamellae from garnet. *American Mineralogist*, *104*, 980–995. https://doi.org/10.2138/am-2019-6849

Keller, D. S., & Ague, J. J. (2020). Quartz, mica, and amphibole exsolution from majoritic garnet reveals ultra-deep sediment

subduction, Appalachian orogen. *Science Advances*, *6*, eaay5178. https://doi.org/10.1126/sciadv.aay5178

Kelly, P. M., & Zhang, M.-X. (2006). Edge-to-edge matching—The fundamentals. *Metallurgical and Materials Transactions A*, *37*, 833–839. https://doi.org/10.1007/s11661-006-0056-4

Kihara, K. (1990). An X-ray study of the temperature dependence of the quartz structure. *European Journal of Mineralogy*, *2*, 63–77. https://doi.org/10.1127/ejm/2/1/0063

Lambert-Perlade, A., Gourges, A. F., & Pineau, A. (2004). Austentite to bainite phase transformation in heat-affected zones of a high strength low alloy steel. *Acta Materialia*, *52*, 2337–2348. https://doi.org/10.1016/j.actamat.2004.01.025

Lin, L. S., Goldstein, J. I., & Williams, D. B. (1979). Analytical electron microscopy study of the plessite structure in four IICD iron meteorites. *Geochimica et Cosmochimica Acta*, *43*, 725–737. https://doi.org/10.1016/0016-7037(79)90256-4

Liu, P., Xie, J., Wang, A., Ma, D., & Mao, Z. (2020). Atomic-scale investigation on the initial precipitation behavior of nitrites in TiAl alloys. *Intermetallics*, *121*, 106777. https://doi.org/10.1016/j.intermet.2020.106777

Liu, S. J., Li, J. H., & Santosh, M. (2010). First application of the revised Ti-in-zircon geothermometer to Paleoproterozoic ultrahigh-temperature granulites of Tuguiwula, Inner Mongolia, North China Craton. *Contributions to Mineralogy and Petrology*, *159*, 225–235. https://doi.org/10.1007/s00410-009-0425-2

Locock, A. J. (2008). An Excel spreadsheet to recast analyses of garnet into end-member components, and a synopsis of the crystal chemistry of natural silicate garnets. *Computers & Geosciences*, *34*, 1769–1780. https://doi.org/10.1016/j.cageo.2007.12.013

Marsh, J. H., & Kelly, E. D. (2017). Petrogenetic relations among titanium-rich minerals in an anatectic high-*P* mafic granulite. *Journal of Metamorphic Geology*, *35*, 717–738. https://doi.org/10.1111/jmg.12252

Meagher, E. P., & Lager, G. A. (1979). Polyhedral thermal expansion in the TiO_2 polymorphs: Refinement of the crystal structures of rutile and brookite at high temperature. *Canadian Mineralogist*, *17*, 77–85.

Miao, Y., Mo, K., Cui, B., Chen, W.-Y., Miller, M. K., Powers, K. A., McCreary, V., Gross, D., Almer, J., Robertson, I. M., & Stubbins, J. F. (2015). The interfacial orientation relationship of oxide nanoparticles in a hafnium-containing oxide dispersion-strengthened austentitic stainless steel. *Materials Characterization*, *101*, 136–143. https://doi.org/10.1016/j.matchar.2015.01.015

Momma, K., & Izumi, F. (2011). VESTA 3 for three-dimensional visualization of crystal, volumetric and morphology data. *Journal of Applied Crystallography*, *44*, 1272–1276. https://doi.org/10.1107/S0021889811038970

Mposkos, E. D., & Kostopoulos, D. K. (2001). Diamond, former coesite and supersilicic garnet in metasedimentary rocks from the Greek Rhodope: A new ultrahigh-pressure metamorphic province established. *Earth and Planetary Science Letters*, *192*, 497–506. https://doi.org/10.1016/S0012-821X(01)00478-2

Nabarro, F. R. N. (1940). The strains produced by precipitation in alloys. *Proceedings of the Royal Society of London a*, *175*, 519–538.

Nesse, W. D. (2011). *Introduction to mineralogy* (2nd ed.). Oxford University Press.

Nolze, G., Geist, V., Saliwan Neumann, R., & Buchheim, M. (2005). Investigation of orientation relationships by EBSD and EDS on the example of the Watson iron meteorite. *Crystal Research and Technology*, *40*, 791–804. https://doi.org/10.1002/crat.200410434

Pearce, M., & Escolme, A. (2021). Phase heritage during replacement reactions in Ti-bearing minerals. *Contributions to Mineralogy and Petrology*, *176*, 21. https://doi.org/10.1007/s00410-021-01775-8

Phillips, D. S., Heuer, A. H., & Mitchell, T. E. (1980a). Precipitation in star sapphire I. Identification of the precipitate. *Philosophical Magazine A*, *42*, 385–404. https://doi.org/10.1080/01418618008239365

Phillips, D. S., Heuer, A. H., & Mitchell, T. E. (1980b). Precipitation in star sapphire II. Elastic accommodation of the precipitate. *Philosophical Magazine A*, *42*, 405–416. https://doi.org/10.1080/01418618008239366

Pollington, A. D., & Baxter, E. F. (2010). High resolution Sm-Nd garnet geochronology reveals the uneven pace of tectonometamorphic processes. *Earth and Planetary Science Letters*, *293*, 63–71. https://doi.org/10.1016/j.epsl.2010.02.019

Proyer, A., Habler, G., Abart, R., Wirth, R., Krenn, K., & Hoinkes, G. (2013). TiO_2 exsolution from garnet by open-system precipitation: Evidence from crystallographic and shape preferred orientation of rutile inclusions. *Contributions to Mineralogy and Petrology*, *166*, 211–234. https://doi.org/10.1007/s00410-013-0872-7

Putnis, A., & John, T. (2010). Replacement processes in the Earth's crust. *Elements*, *6*, 159–164. https://doi.org/10.2113/gselements.6.3.159

Putnis, A., & Putnis, C. V. (2007). The mechanism of reequilibration of solids in the presence of a fluid phase. *Journal of Solid State Chemistry*, *180*, 1783–1786. https://doi.org/10.1016/j.jssc.2007.03.023

Qiu, D., Zhang, M.-X., Fu, H.-M., Kelly, P. M., & Taylor, J. A. (2007). Crystallography of recently developed grain refiners for Mg–Al alloys. *Philosophical Magazine Letters*, *87*, 505–514. https://doi.org/10.1080/09500830701253151

Robinson, P., Ross, M., Nord, G. L. Jr., Smyth, J. R., & Jaffe, H. W. (1977). Exsolution lamellae in augite and pigeonite: Fossil indicators of lattice parameters at high temperature and pressure. *American Mineralogist*, *62*, 857–873.

Rodehorst, U., Geiger, C. A., & Armbruster, T. (2002). The crystal structures of grossular and spessartine between 100 and 600 K and the chemistry of grossular-spessartine solid solutions. *American Mineralogist*, *87*, 542–549. https://doi.org/10.2138/am-2002-0417

Rogowitz, A., & Huet, B. (2021). Evolution of fluid pathways during eclogitization and their impact on formation and deformation of eclogite: A microstructural and petrological investigation at the type locality (Koralpe, eastern Alps, Austria). *Tectonophysics*, *819*, 229079. https://doi.org/10.1016/j.tecto.2021.229079

Russell, K. C. (1980). Nucleation in solids: The induction and steady state effects. *Advances in Colloid and Interface Science*, *13*, 205–318. https://doi.org/10.1016/0001-8686(80)80003-0

Sakamaki, K., Sato, Y., & Ogasawara, Y. (2016). Hydrous Na-garnet from garnet ridge; products of mantle metasomatism underneath the Colorado plateau. *Progress in Earth and Planetary Science*, *3*, 20. https://doi.org/10.1186/s40645-016-0095-4

Sánchez-Muñoz, L., del Campo, A., & Fernández, J. F. (2016). Symmetry constraints during the development of anisotropic spinodal patterns. *Scientific Reports*, *6*(20806), 1–10. https://doi.org/10.1038/srep20806

Servi, I. S., & Turnbull, D. (1966). Thermodynamics and kinetics of precipitation in the copper-cobalt system. *Acta Metallurgica*, *14*, 161–169. https://doi.org/10.1016/0001-6160(66)90297-5

Shewmon, P. G. (1969). Transformations in metals. *McGraw-Hill*, 1–394.

Shiflet, G. J., & van der Merwe, J. H. (1994). The role of structural ledges as misfit-compensating defects: fcc-bcc interphase boundaries. *Metallurgical and Materials Transactions a*, *25*, 1895–1903. https://doi.org/10.1007/BF02649037

Shinevar, W. J., Jagoutz, O., & VanTongeren, J. A. (2021). Gore Mountain garnet amphibolite records UHT conditions: Implications for the rheology of the lower continental crust during orogenesis. *Journal of Petrology*, *62*(4), egab007. https://doi.org/10.1093/petrology/egab007

Smith, D. A., & Shiflet, G. (1987). Low energy dislocation structures in interfaces. *Materials Science and Engineering*, *86*, 67–92.

Song, S., Zhang, L., Chen, J., Liou, J. G., & Niu, Y. (2005). Sodic amphibole exsolutions in garnet from garnet-peridotite, North Qaidam UHPM belt, NW China: Implications for ultradeep-origin and hydroxyl defects in mantle garnets. *American Mineralogist*, *90*, 814–820. https://doi.org/10.2138/am.2005.1684

Spengler, D. (2006). *Origin and evolution of deep upper mantle rocks from Western Norway* [Ph.D. Thesis]. University of Utrecht.

Spengler, D., Alifirova, T. A., & van Roermund, H. L. M. (2021). Subcratonic and tectonic evolution of pyroxenite and eclogite with lamellar inclusions in garnet, Western gneiss region, Norway. *Journal of Petrology*, *62*(8), egab008. https://doi.org/10.1093/petrology/egab008

Stanford, N., & Bate, P. S. (2005). Crystallographic variant selection in α–β brass. *Acta Materialia*, *53*, 859–867. https://doi.org/10.1016/j.actamat.2004.10.043

Swamy, V., Saxena, S. K., Sundman, B., & Zhang, J. (1994). A thermodynamic assessment of silica phase diagram. *Journal of Geophysical Research*, *99*, 11787–11794. https://doi.org/10.1029/93JB02968

Tassara, S., Ague, J. J., & Valencia, V. (2021). The deep magmatic cumulate roots of the Acadian orogen, eastern North America. *Geology*, *49*, 168–173. https://doi.org/10.1130/G47887.1

Thiéblot, L., Roux, J., & Richet, P. (1998). High-temperature thermal expansion and decomposition of garnets. *European Journal of Mineralogy*, *10*, 7–15. https://doi.org/10.1127/ejm/10/1/0007

Thomas, J. B., & Nachlas, W. O. (2020). Discontinuous precipitation of rutilated quartz: Grain-boundary migration induced by changes to the equilibrium solubility of Ti in quartz. *Contributions to Mineralogy and Petrology*, *175*, 38. https://doi.org/10.1007/s00410-020-01676-2

van der Merwe, J. H. (1978). The role of lattice misfit in epitaxy. *Critical Reviews in Solid State and Materials Sciences*, *7*, 209–231. https://doi.org/10.1080/10408437808243439

van Roermund, H. L. M., & Drury, M. R. (1998). Ultra-high pressure ($P > 6$ GPa) garnet peridotites in Western Norway: Exhumation of mantle rocks from >185 km depth. *Terra Nova*, *10*, 295–301. https://doi.org/10.1046/j.1365-3121.1998.00213.x

van Roermund, H. L. M., Drury, M. R., Barnhoorn, A., & de Ronde, A. (2000). Non-silicate inclusions in garnet from an ultra-deep orogenic peridotite. *Geological Journal*, *35*, 209–229. https://doi.org/10.1002/gj.858

Wang, L., Essene, E. J., & Zhang, Y. (1999). Mineral inclusions in pyrope crystals from Garnet Ridge, Arizona, USA: Implications for processes in the upper mantle. *Contributions to Mineralogy and Petrology*, *135*, 164–178. https://doi.org/10.1007/s004100050504

Weatherly, G. C. (1971). The structure of ledges at plate-shaped precipitates. *Acta Metallurgica*, *19*, 181–192. https://doi.org/10.1016/0001-6160(71)90145-3

Weatherly, G. C., & Nicholson, R. B. (1968). An electron microscope investigation of the interfacial structure of semi-coherent precipitates. *Philosophical Magazine*, *17*, 801–831. https://doi.org/10.1080/14786436808223031

Wechsler, B. A., & Prewitt, C. T. (1984). Crystal structure of ilmenite ($FeTiO_3$) at high temperature and at high pressure. *American Mineralogist*, *69*, 176–185.

Whitney, D. L., & Evans, B. W. (2010). Abbreviations for names of rock-forming minerals. *American Mineralogist*, *95*, 185–187. https://doi.org/10.2138/am.2010.3371

Wilson, R. N., & Partridge, P. G. (1965). The nucleation and growth of S' precipitates in an aluminum-2.5% copper-1.2% magnesium alloy. *Acta Metallurgica*, *13*, 1321–1327. https://doi.org/10.1016/0001-6160(65)90043-X

Winkelman, G. B., Raviprasad, K., & Muddle, B. C. (2007). Orientation relationships and lattice matching for the S phase in Al–Cu–Mg alloys. *Acta Materialia*, *55*, 3213–3228. https://doi.org/10.1016/j.actamat.2007.01.011

Xu, H. J., & Wu, Y. (2017). Oriented inclusions of pyroxene, amphibole, and rutile in garnet from the Lüliangshan garnet peridotite massif, North Qaidam UHPM belt, NW China: An electron backscatter diffraction study. *Journal of Metamorphic Geology*, *35*, 1–17.

Ye, K., Cong, B., & Ye, D. (2000). The possible subduction of continental material to depths greater than 200 km. *Nature*, *407*, 734–736. https://doi.org/10.1038/35037566

Zhang, J. F., Xu, H. J., Liu, Q., Green, H. W. II, & Dobrzhinetskaya, L. F. (2011). Pyroxene exsolution topotaxy in majoritic garnet from 250 to 300 km depth. *Journal of Metamorphic Geology*, *29*, 741–751. https://doi.org/10.1111/j.1525-1314.2011.00939.x

Zhang, M.-X., & Kelly, P. M. (1998). Crystallography and morphology of Widmanstätten cementite in austentite. *Acta Materialia*, *46*, 4617–4628. https://doi.org/10.1016/S1359-6454(98)00139-6

Zhang, M.-X., & Kelly, P. M. (2005). Edge-to-edge matching model for predicting orientation relationships and habit planes—The improvements. *Scripta Materialia*, *52*, 963–968. https://doi.org/10.1016/j.scriptamat.2005.01.040

Zhang, R. Y., & Liou, J. G. (1999). Exsolution lamellae in minerals from ultrahigh-pressure rocks. *International Geology Review*, *41*, 981–993. https://doi.org/10.1080/00206819909465184

Zhong, N., Wang, X., Guo, Z., & Rong, Y. (2011). Orientation relationships between ferrite and cementite by edge-to-edge matching principle. *Journal of Materials Science and Technology*, *27*, 475–480. https://doi.org/10.1016/S1005-0302(11)60094-7

SUPPORTING INFORMATION

Additional supporting information may be found in the online version of the article at the publisher's website.

Table S1. Unit cell parameters of garnet and select precipitate species at low and high temperature

Table S2. Mismatch (Å) between low-index structural elements for enstatite and garnet for two garnet compositions

Table S3. Mismatch (Å) between low-index structural elements for diopside and garnet for two garnet compositions

How to cite this article: Keller, D. S., & Ague, J. J. (2022). Predicting and explaining crystallographic orientation relationships of exsolved precipitates in garnet using the edge-to-edge matching model. *Journal of Metamorphic Geology*, *40*(7), 1189–1218. https://doi.org/10.1111/jmg.12662